

University of Groningen

Photometry and models of selected main belt asteroids. IX. Introducing interactive service for asteroid models (ISAM)

Marciniak, A.; Bartczak, P.; Santana-Ros, T.; Michalowski, T.; Antonini, P.; Behrend, R.; Bembrick, C.; Bernasconi, L.; Borczyk, W.; Colas, F.

Published in:
Astronomy & astrophysics

DOI:
[10.1051/0004-6361/201219542](https://doi.org/10.1051/0004-6361/201219542)

IMPORTANT NOTE: You are advised to consult the publisher's version (publisher's PDF) if you wish to cite from it. Please check the document version below.

Document Version
Publisher's PDF, also known as Version of record

Publication date:
2012

[Link to publication in University of Groningen/UMCG research database](#)

Citation for published version (APA):

Marciniak, A., Bartczak, P., Santana-Ros, T., Michalowski, T., Antonini, P., Behrend, R., ... Zafar, T. (2012). Photometry and models of selected main belt asteroids. IX. Introducing interactive service for asteroid models (ISAM). *Astronomy & astrophysics*, 545, [A131]. <https://doi.org/10.1051/0004-6361/201219542>

Copyright

Other than for strictly personal use, it is not permitted to download or to forward/distribute the text or part of it without the consent of the author(s) and/or copyright holder(s), unless the work is under an open content license (like Creative Commons).

Take-down policy

If you believe that this document breaches copyright please contact us providing details, and we will remove access to the work immediately and investigate your claim.

Downloaded from the University of Groningen/UMCG research database (Pure): <http://www.rug.nl/research/portal>. For technical reasons the number of authors shown on this cover page is limited to 10 maximum.

Photometry and models of selected main belt asteroids

IX. Introducing interactive service for asteroid models (ISAM)^{★,★★}

A. Marciniak¹, P. Bartczak¹, T. Santana-Ros¹, T. Michałowski¹, P. Antonini², R. Behrend³, C. Bembrick⁴, L. Bernasconi⁵, W. Borczyk¹, F. Colas⁶, J. Coloma⁷, R. Crippa⁸, N. Esseiva⁹, M. Fagas¹, M. Fauvaud¹⁰, S. Fauvaud¹⁰, D. D. M. Ferreira¹¹, R. P. Hein Bertelsen¹², D. Higgins¹³, R. Hirsch¹, J. J. E. Kajava¹⁴, K. Kamiński¹, A. Kryszczyńska¹, T. Kwiatkowski¹, F. Manzini⁸, J. Michałowski¹⁵, M. J. Michałowski¹⁶, A. Paschke¹⁷, M. Polińska¹, R. Poncy¹⁸, R. Roy¹⁹, G. Santacana⁹, K. Sobkowiak¹, M. Stasik¹, S. Starczewski²⁰, F. Velichko²¹, H. Wucher⁹, and T. Zafar²²

¹ Astronomical Observatory Institute, Faculty of Physics, A. Mickiewicz University, Słoneczna 36, 60-286 Poznań, Poland
e-mail: aniab@lab.astro.amu.edu.pl

² Observatoire de Bédoine, 47 rue Guillaume Puy, 84000 Avignon, France

³ Geneva Observatory, 1290 Sauverny, Switzerland

⁴ Bathurst, NSW, Australia

⁵ Les Engarouines Observatory, 84570 Mallemort-du-Comtat, France

⁶ IMCCE, Paris Observatory, UMR 8028, CNRS, 77 av. Denfert-Rochereau, 75014 Paris, France

⁷ Agrupación Astronómica de Sabadell, Apartado de Correos 50, PO Box 50, 08200 Sabadell, Barcelona, Spain

⁸ Stazione Astronomico di Sozzago, 28060 Sozzago, Italy

⁹ Association AstroQueyras, 05350 Saint-Véran, France

¹⁰ Observatoire du Bois de Bardon, 16110 Taponnat, France

¹¹ DTU Space, Technical University of Denmark, Juliane Maries Vej 30, 2200 Copenhagen, Denmark

¹² Kapteyn Astronomical Institute, University of Groningen, PO box 800, 9700 AV Groningen, The Netherlands

¹³ Canberra, ACT, Australia

¹⁴ Astronomy Division, Department of Physics, PO Box 3000, 90014 University of Oulu, Finland

¹⁵ Forte Software, Os. Jagieły 28/28, 60-694 Poznań, Poland

¹⁶ SUPA***, Institute for Astronomy, University of Edinburgh, Royal Observatory, Edinburgh, EH9 3HJ, UK

¹⁷ Groupe européen d'observation stellaire (GEOS), 23 Parc de Levesville, 28300 Bailleau l'Evêque, France

¹⁸ 2 rue des Ecoles, 34920 Le Crès, France

¹⁹ Blaauw Observatory, 84570 St-Estève, France

²⁰ N. Copernicus Astronomical Centre, Polish Academy of Sciences, Bartycka 18, 00-716 Warsaw, Poland

²¹ Institute of Astronomy, Karazin Kharkiv National University, Sums'ka 35, 61022 Kharkiv, Ukraine

²² Laboratoire d'Astrophysique de Marseille, OAMP, Université Aix-Marseille & CNRS, 38 rue Frederic Joliot Curie, 13388 Cedex 13, France

Received 4 May 2012 / Accepted 12 July 2012

ABSTRACT

Context. The shapes and spin states of asteroids observed with photometric techniques can be reconstructed using the lightcurve inversion method. The resultant models can then be confirmed or exploited further by other techniques, such as adaptive optics, radar, thermal infrared, stellar occultations, or space probe imaging.

Aims. During our ongoing work to increase the set of asteroids with known spin and shape parameters, there appeared a need for displaying the model plane-of-sky orientations for specific epochs to compare models from different techniques. It would also be instructive to be able to track how the complex lightcurves are produced by various asteroid shapes.

Methods. Basing our analysis on an extensive photometric observational dataset, we obtained eight asteroid models with the convex *lightcurve inversion* method. To enable comparison of the photometric models with those from other observing/modelling techniques, we created an on-line service where we allow the inversion models to be orientated interactively.

Results. Our sample of objects is quite representative, containing both relatively fast and slow rotators with highly and lowly inclined spin axes. With this work, we increase the sample of asteroid spin and shape models based on disk-integrated photometry to over 200. Three of the shape models obtained here are confirmed by the stellar occultation data; this also allowed independent determinations of their sizes to be made.

Conclusions. The ISAM service can be widely exploited for past and future asteroid observations with various, complementary techniques and for asteroid dimension determination.

Key words. techniques: photometric – minor planets, asteroids: general

* <http://isam.astro.amu.edu.pl>

** Photometric data are only available at the CDS via anonymous ftp to cdsarc.u-strasbg.fr (130.79.128.5) or via

<http://cdsarc.u-strasbg.fr/viz-bin/qcat?J/A+A/545/A131>

*** Scottish Universities Physics Alliance.

1. Introduction

Asteroids observed at various viewing and illumination geometries can be uniquely modelled with the *lightcurve inversion* method (Kaasalainen et al. 2001). The observed light variations

can be in the form of both traditional dense lightcurves and calibrated datapoints distributed sparsely in time. The resulting model consists of the convex shape representation and the spin parameters of the sidereal period and spin axis orientation. Other observing techniques such as stellar occultations by asteroids, adaptive optics imaging, radar echo, or thermal infrared technique can yield or exploit detailed shape models. To obtain as much shape details as possible, we decided to focus on asteroid modelling based on low-scatter dense lightcurves.

A comparison of the inversion models with the adaptive optics technique was successfully made in, e.g., Marchis et al. (2006). In most cases, this allowed the rejection of the mirror pole solution, and the shape outline was confirmed. We performed another comparison in Marciniak et al. (2011), that confirmed one of the pole and shape solutions for asteroid (679) Pax.

Since stellar occultations by asteroids are being observed nowadays more extensively and accurately than ever before (see Dunham et al. 2011)¹, it has become possible to overlay the occultation shadow chords and the photometric asteroid model (see Timerson et al. 2009; or Ďurech et al. 2011). This can confirm the shape model and distinguish which of the pole solutions is correct. However, there has been no interactive tool that could be used to perform a straightforward orientation of the asteroid models in the plane of sky for a given moment (though the physical ephemeris can be obtained with the Virtual Observatory service², Berthier et al. 2008). Spin and shape models obtained from photometric techniques are being gathered in the DAMIT database³ (Ďurech et al. 2010).

To enable comparison of the photometric models with those from other observing or modelling techniques, we created an online service where we allow the orientation of these models to be determined interactively. Moreover, we present new photometric observations and physical models of asteroids (76) Freia, (127) Johanna, (355) Gabriella, (386) Siegena, (417) Suevia, (435) Ella, (505) Cava, and (699) Hela. In cases when data from stellar occultations are available, we compare our shape models to the occultation profiles. This allows us to calibrate the asteroid size, and provides the pole and shape confirmation.

2. Observations

We gathered data from our continuing main-belt asteroid observations at the Borowiec station of the Poznań Astronomical Observatory (see Michałowski et al. 2004), and from other observatories, both amateur and professional. This joint effort allowed us to obtain a larger than usual sample of asteroid spin and shape models based exclusively on dense lightcurves. This sample of eight asteroids should crucially be free of common biases, containing both relatively fast and slow rotators ($P = 3$ to 12 h) and high and low spin-axis inclinations with respect to the ecliptic plane ($|\beta_p|$ from 10 to 88 degrees). There are also large (200 km in diameter) and relatively small (13 km) objects in our sample of main-belt asteroids.

The total number of lightcurves used in our modelling was 248, 199 of which were new lightcurves and the remaining ones taken from SAPC⁴, ALCDEF⁵, or provided by the authors themselves.

Table 2. Asteroid parameters.

Asteroid	D [km]	Albedo	Type	a [AU]	e	i [$^\circ$]	Ω [$^\circ$]
(76) Freia	168	0.043	C	3.4159	0.163	2.12	204.51
(127) Johanna	114	0.065	Ch	2.7549	0.065	8.24	31.22
(355) Gabriella	25	0.207	S	2.5375	0.106	4.28	351.89
(386) Siegena	201	0.047	Ch	2.8964	0.173	20.26	166.92
(417) Suevia	50	0.134	X	2.8047	0.132	6.62	199.68
(435) Ella	37	0.106	DCX	2.4497	0.155	1.82	23.26
(505) Cava	100	0.063	FC	2.6851	0.245	9.84	90.92
(699) Hela	13	0.203	Sk	2.6163	0.407	15.30	242.73

Notes. See page footnotes 6 and 7 for the source references.

The data are presented in a form of composite lightcurves (Figs. 21–67, see Appendix). They can be obtained from both the CDS and DAMIT databases. Table 1 (see Appendix) contains the aspect data for all the observing runs. The mid-time of the observing run and the distances to the Earth and Sun in astronomical units are indicated in the first three columns. The table also shows the corresponding Sun-object-Earth phase angle and the J2000 ecliptic latitude and longitude of an asteroid in the sky. The next two columns give the number of points in each lightcurve and an estimate of the observational quality, which we estimated using the dispersion in the corresponding magnitude difference between two comparison stars, where such information was available. The last column provides the observatory code.

Table 2 contains the physical characteristics of these asteroids, including their effective diameters, geometric albedoes, taxonomic types, and orbital parameters^{6,7}.

3. Photometry and models

We briefly describe earlier results on the selected targets, summarise the general character of their light variations, and describe our models with an outline of the modelling process. The *lightcurve inversion* method used here is described in Kaasalainen & Torppa (2001) and Kaasalainen et al. (2001). Table 3 contains the obtained spin parameters, their error values estimated from the parameter space, and a comparison to previous results. After the sidereal period value, there are λ_p, β_p J2000 ecliptic coordinates of the spin-axis pole solutions, usually with an inevitable mirror pair of values. Since the error values were similar for both solutions, we cannot point at any of two poles as preferred. The next few columns of Table 3 give the overall number of apparitions (N_{app}) when an asteroid was observed, the number of separate lightcurves (N_{lc}) used for modelling, the method used (“A” stands for amplitude, “M” – magnitude, “E” – epoch, and “L” – lightcurve inversion methods), and the reference. The shape models and their example lightcurves compared to data are shown in Figs. 1 to 16.

⁶ Data for these properties come from *The Small Bodies Node of the NASA Planetary Data System* <http://pdssbn.astro.umd.edu/>), where the diameters and albedos are mainly from the asteroid catalogue using AKARI Ver. 1.0 (Usui et al. 2011), and the taxonomic classifications are given after Bus & Binzel (2002).

⁷ The data on orbital parameters come from the Minor Planet Center database available at:
<ftp://cfa-ftp.harvard.edu/pub/MPCORB/MPCORB.DAT>

¹ <http://sbn.psi.edu/pds/resource/occ.html>

² <http://vo.imcce.fr/webservices/miriade/?ephemph>

³ <http://astro.troja.mff.cuni.cz/projects/asteroids3D>

⁴ <http://asteroid.astro.helsinki.fi/apc>

⁵ http://minorplanetcenter.net/light_curve

Table 3. Parameters of the models with their estimated error values.

Sidereal period (hours)	Pole 1		Pole 2		Observing span (years)	N_{app}	N_{lc}	Method	Reference
	λ_p	β_p	λ_p	β_p					
(76) Freia									
9.968286	139°	+25	0°	+40°	1981–2007	4	13	L	Stephens & Warner (2008)
9.973061	139°	+14	320°	+17°	1981–2010	8	38	L	Present work
±0.000005	±2°	±1°	±2°	±1°					
(127) Johanna									
12.79954	98°	-59	261°	-69°	1982–2011	8	33	L	Present work
±0.00002	±5°	±5°	±25°	±5°					
(355) Gabriella									
4.82899	164°	+78	332°	+71°	1992–2004	1*	4	L(com)	Ďurech (2006)
4.82899			0°	+69°	1992–2004	1*	4	L(com)	Ďurech et al. (2009)
4.82899	197°	+70	341°	+78°	1992–2004	1*	4	L(com)	Hanuš et al. (2011)
4.828994	159°	+88	341°	+83°	1992–2010	5	16	L	Present work
±0.000001	±20°	±10°	±20°	±10°					
(386) Siegena									
	56°	+14	236°	-14°	1979–1980	2	10	AM	Blanco & Riccioli (1998)
9.76503	104°	-10	289°	+25°	1979–2010	10	60	L	Present work
±0.00001	±2°	±4°	±1°	±4°					
(417) Suevia									
7.01848	13°	+23	186°	+20°	1989–2010	7	37	L	Present work
±0.00001	±2°	±2°	±2°	±2°					
(435) Ella									
4.622802	59°	+64	247°	+58°	1986–2011	7	18	L	Present work
±0.000001	±5°	±5°	±5°	±5°					
(505) Cava									
	113°	4°	239°	-10°	1975–1982	3	11	Z	Young & Harris (1985)
	138°	+40	325°	+27°	1979–1993	3	11	EAM	Michałowski (1996)
8.180050	131°	-21	304°	-44°	1979–2010	8	40	L	Present work
±0.000003	±5°	±5°	±5°	±5°					
(699) Hela									
3.396232	45°	+44	197°	+31°	1982–2011	7	21	L	Present work
±0.000001	±5°	±5°	±2°	±2°					

Notes. See Sect. 3 for a description of the columns of this table. * Combined sparse + dense data.

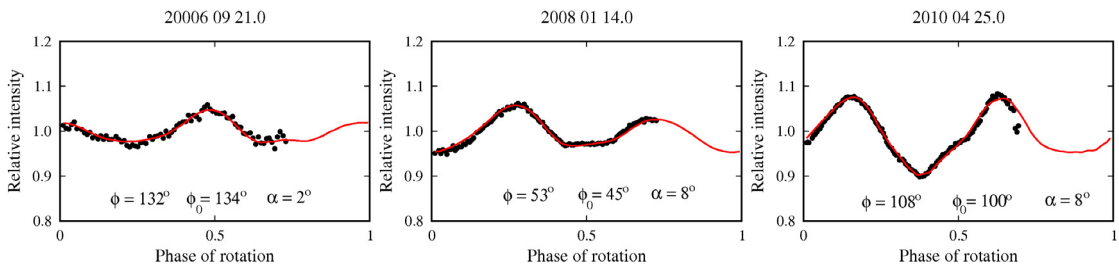


Fig. 1. Observed lightcurves (points) superimposed on the model lightcurves (lines) at the same epochs for (76) Freia. The overall root mean square (rms) residual of the fit was 0.0120 mag.

3.1. (76) Freia

The first photometric observations of (76) Freia were performed by Harris & Young (1983) in 1979, yielding a synodic period value of 9.79 h. Further observations were obtained in 1981 by Lagerkvist et al. (1987) and Harris et al. (1992). The latter work reported a synodic period of 9.972 h. In 1984, (76) Freia was observed again, with a determined period of 9.98 h (Lagerkvist et al. 1986).

Publications that also contain data on this asteroid include Armstrong et al. (1996), Kryszczyńska et al. (1996), and Shevchenko et al. (2005, 2008), where synodic periods from 9.97 to 9.994 h are reported. All these results show that this rather long-period and low-amplitude asteroid exhibits regular, bimodal lightcurves.

Stephens & Warner (2008) obtained a preliminary model of (76) Freia using the *lightcurve inversion* method, for a dataset of 13 separate lightcurves from four apparitions (see Table 3).

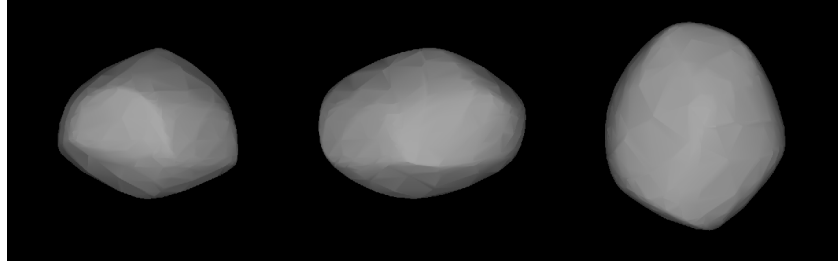


Fig. 2. Convex shape model “2” of (76) Freia, shown at equatorial viewing and illumination geometry, with rotational phases 90° apart (two pictures on the *left*), and the pole-on view at the *right*. The reflectivity law is artificial, to reveal the shape details.

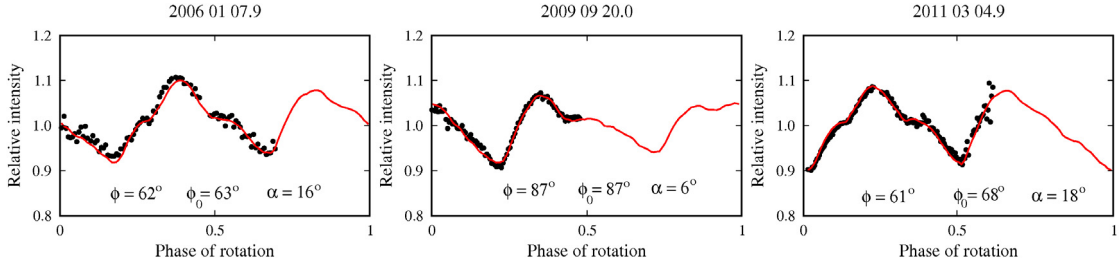


Fig. 3. Observed vs. modelled lightcurves for (127) Johanna. The rms residual of the fit was 0.0127 mag.

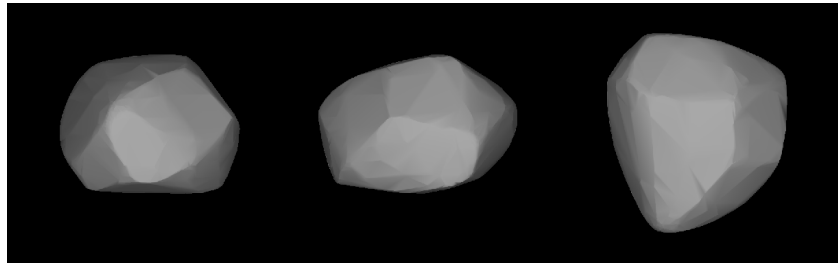


Fig. 4. Shape model “2” of (127) Johanna.

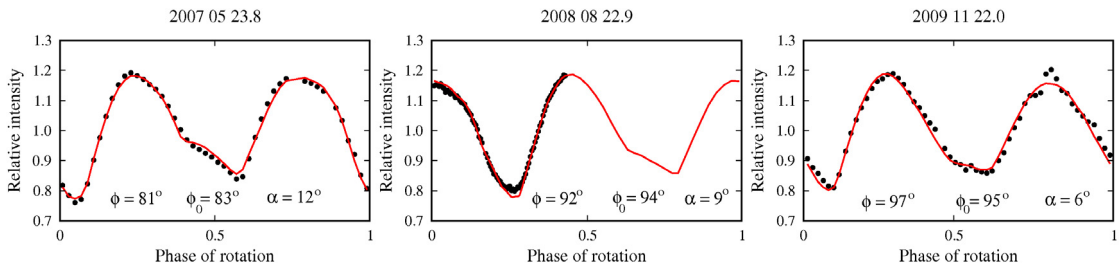


Fig. 5. Observed vs. modelled lightcurves for (355) Gabriella. The rms residual of the fit was 0.0226 mag.

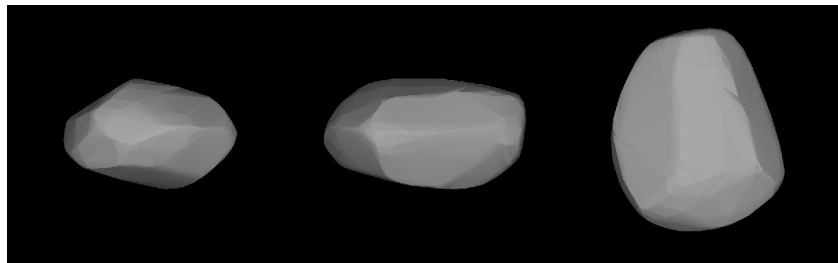


Fig. 6. Shape model “2” of (355) Gabriella.

We observed Freia during five apparitions (see Table 1 for dates and other information about the observing runs). The synodic period that fitted all of the apparitions was 9.974 h,

which is identical to the Shevchenko et al. (2005) determination. Figures 21 to 25 (see Appendix) show our observations in the form of composite lightcurves with the model orientation at the

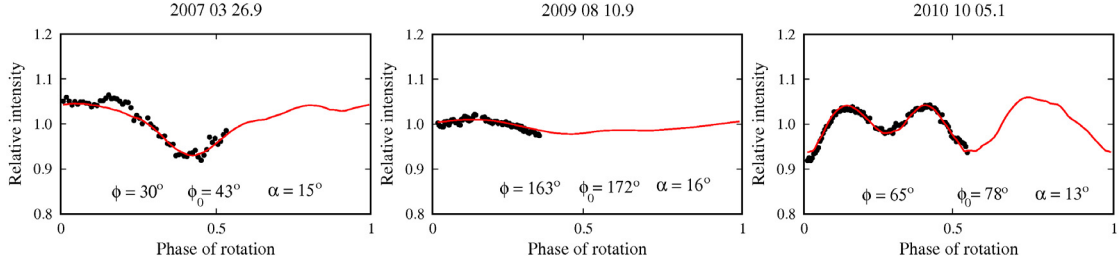


Fig. 7. Observed vs. modelled lightcurves for (386) Siegena. The rms residual of the fit was 0.0083 mag.

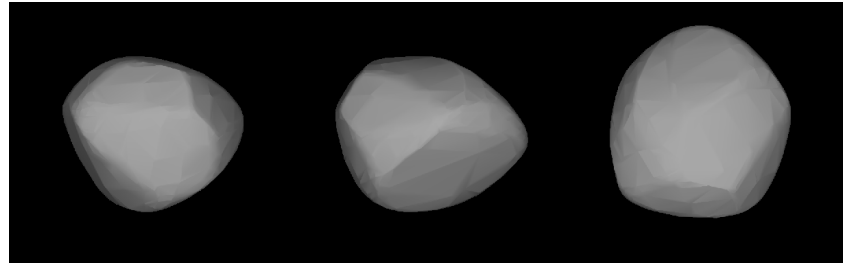


Fig. 8. Shape model “2” of (386) Siegena.

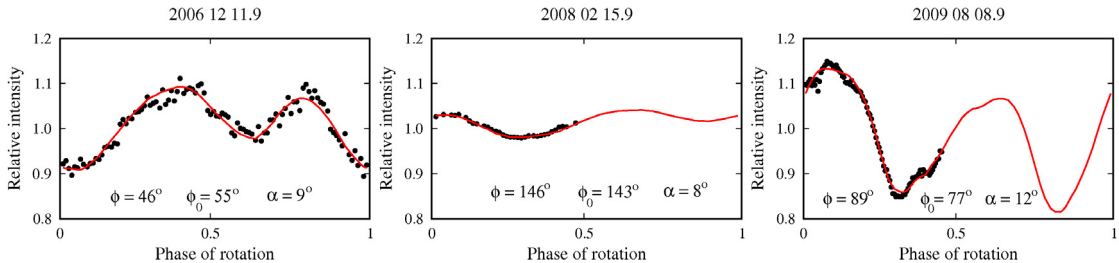


Fig. 9. Observed vs. modelled lightcurves for (417) Suevia. The rms residual of the fit was 0.0165 mag.

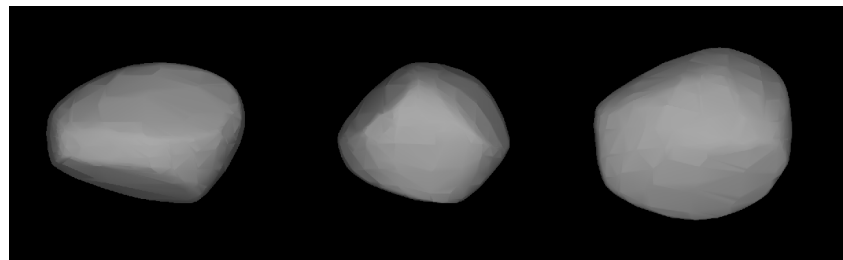


Fig. 10. Shape model “2” of (417) Suevia.

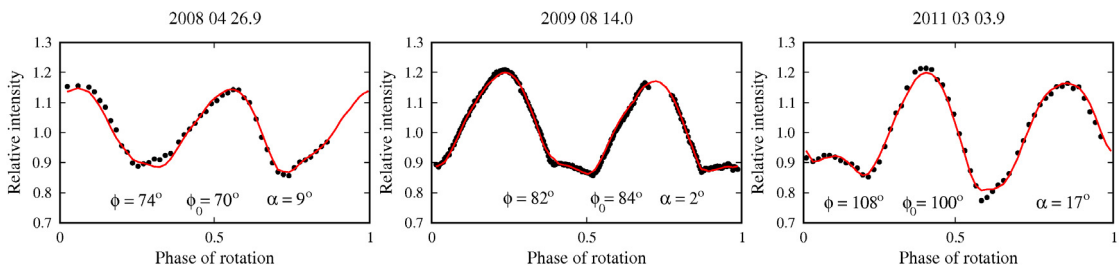


Fig. 11. Observed vs. modelled lightcurves for (435) Ella. The rms residual of the fit was 0.0153 mag.

zero time. The amplitudes were smallest in the 2002 apparition (0.06 mag), and greatest in 2010 (0.20 mag). Characteristic flat minima could be seen in some of the apparitions.

Obtaining a unique solution for the spin/shape model of Freia was surprisingly difficult. We could not find a unique sidereal period, even with our large dataset. Only by modifying the

initial period-scanning procedure and enlarging the number of 6 initial poles to 12, did we find the best-fit model for both spin-axis orientation and period. We created the final model for 38 lightcurves from 8 apparitions (see Table 3 for the best-fit model parameters and their error values). The spin pole position is defined with very small uncertainty, but the z-axis dimension

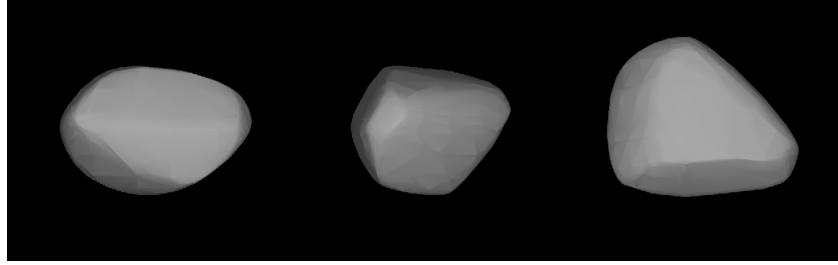


Fig. 12. Shape model “1” of (435) Ella.

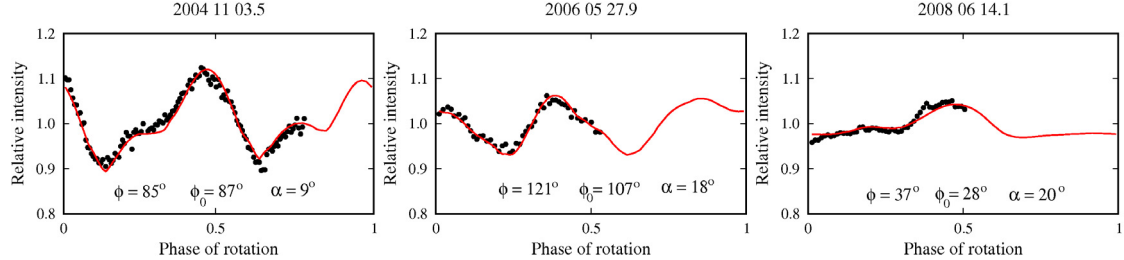


Fig. 13. Observed vs. modelled lightcurves for (505) Cava. The rms residual of the fit was 0.0122 mag.

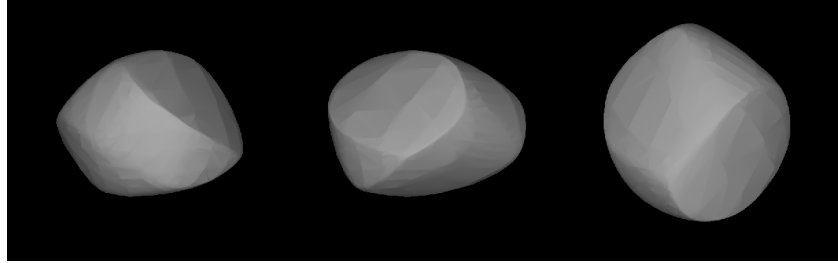


Fig. 14. Shape model “1” of (505) Cava.

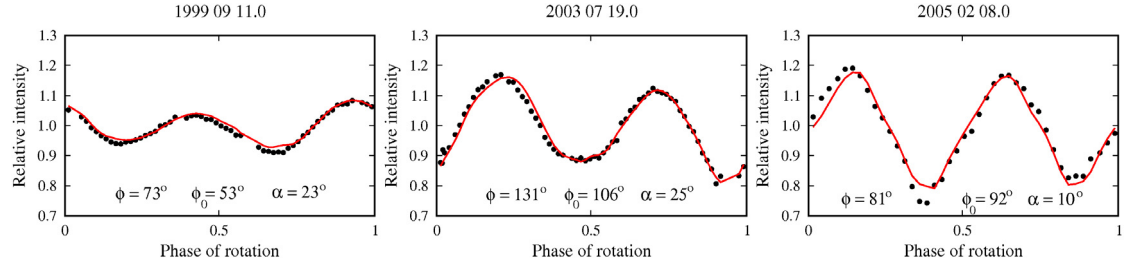


Fig. 15. Observed vs. modelled lightcurves for (699) Hela. The rms residual of the fit was 0.0287 mag.



Fig. 16. Shape model “2” of (699) Hela.

of the shape model is poorly constrained. Figures 2 and 1 display one of two shape models and its fit to the observed lightcurves. Our model differs substantially from that of Stephens & Warner (2008) in terms of the sidereal period value, but agrees with one of their pole solutions. A much larger dataset and improved modelling method would ensure that the model presented here was

more reliable. The same applies to the remaining models differing from the previous solutions presented Table 3. In addition, the error values, which here usually do not exceed $\pm 5^\circ$ indicate that the lightcurve inversion method on dense lightcurves is superior to the classical E, A, and M methods, where the spin poles were usually only accurate to $\pm 20^\circ$.

3.2. (127) Johanna

There are only two previous papers with observations of this asteroid's light variations. The first one, by Harris et al. (1999), contains data from 1982 and a suggestion of a period of around 11 h, based on one fragmentary lightcurve. The other one, by Toth (1997), reports on observations of (127) Johanna taken in 1991. Many short fragments of the lightcurve were folded with a period of 6.94 h, which is much shorter than the previous determination.

We have been gathering data on Johanna since 1997, which resulted in 37 individual lightcurves coming from eight apparitions and a precise synodic period value of 12.7976 h. Composite lightcurves shown in Figs. 26 to 32 (see Appendix) have asymmetric maxima and a steady amplitude of around 0.20 mag. Our observing runs were long and extensive enough to pinpoint the right synodic period value, thus resolving previous ambiguities.

During the modelling with the *lightcurve inversion*, we were unable to obtain a model fitting of all the available lightcurves simultaneously. After rejecting all the data from 1991 and 1997, the model fit immediately improved, while the final model parameters remained almost the same, only now they were much tighter in the parameter space than before. This effect is usually seen when adding more data, while here it happened after discarding discrepant data. The final model was created on 33 lightcurves from 8 apparitions (see Table 3). The second solution for the pole, being much "higher" implies that there is larger uncertainty in a pole longitude than the first one. Figures 4 and 3 present one of two obtained shape models and its fit to three example lightcurves.

3.3. (355) Gabriella

Di Martino et al. (1994) observed (355) Gabriella in 1992, obtaining 0.35 mag amplitude lightcurves, and a 4.830 h period. There are three available spin and shape solutions based on combined sparse + dense datasets by Ďurech (2006), Ďurech et al. (2009), and Hanuš et al. (2011) (see Table 3), all placing the pole far from the ecliptic plane.

Beginning in the year 2005, both professional and amateur observations enlarged the dataset to 16 lightcurves from five apparitions, enabling us to obtain a unique model based on dense lightcurves. In these observations, Gabriella displayed high amplitude lightcurves (up to 0.60 mag, depending on a phase angle) with asymmetric minima (Figs. 33 to 36, see Appendix).

Interestingly, even though apparitions were placed in only four distinct places on the asteroid's orbit, a unique model was found without a problem. Owing to the high albedo of this object, a Lambertian part of the light scattering by the model had to be increased in order to obtain realistic shape models (Fig. 6). Figure 5 shows some of the lightcurve fits. Our model is close to the previous determinations in the sidereal period and, to a lesser extent, in the spin axis position (Table 3). The pole presented here is closer to the pole of the ecliptic, and two obtained solutions may actually be one, which is almost perpendicular to the ecliptic plane.

3.4. (386) Siegena

The first photometric observations of (386) Siegena come from 1979 (Harris & Young 1983) and 1980 (Zappala et al. 1982). The latter paper determined the period to be 9.763 h. Stephens (2005) gives a period of 15.98 h based on new data gathered in

2004, but corrects the value to 9.760 h in 2007 (Stephens 2007), thus confirming the period derived by Zappala et al. Blanco & Riccioli (1998) made a preliminary pole determination using the amplitude-magnitude method (see Table 3), which was not confirmed by our results.

We observed Siegena during 8 apparitions. Unfortunately, some of them happened in the same places in its orbit (see Table 1, in Appendix). The composite lightcurves in Figs. 37 to 44 (Appendix) display rather small amplitudes of from 0.08 mag to 0.19 mag, and the minima at different levels. The synodic period fitting all the apparitions was 9.765 h, which is close to two of the previous determinations.

The best-fit sidereal period could only be found during a higher spatial-resolution scan of the initial poles (as in the case of (76) Freia). The modelling was also complicated by noisy lightcurves from the 1999 and 2004 apparitions. After excluding the most noisy lightcurves from these years, a unique model was found for 60 lightcurves from 10 apparitions, placed at six distinct positions along the ecliptic longitude. There are two strong, but narrow solutions for the pole in the parameter space (Table 3). The preferred shape model and its lightcurve fits are presented in Figs. 8 and 7.

3.5. (417) Suevia

The only published Suevia lightcurve observations are those of Barucci et al. (1992). They were performed in 1989 and the authors determined a period of 7.034 h.

Our data span six apparitions and are displayed in Figs. 45–50. The lightcurves show changes that are typical of an asteroid that has a low-lying pole with respect to the ecliptic. We detected both relatively large (0.37 mag) and small (0.07 mag) amplitudes, and the synodic period was 7.019 h, which is close to the determination of Barucci et al. (1992).

Our lightcurve inversion model of Suevia was based on 37 lightcurves from 7 apparitions. Although scanning possible sidereal period values gives a few possibilities in addition to the best-fitting one, only this period solution (see Table 3) provides physical shape models (Fig. 10) and good lightcurve fits (Fig. 9).

3.6. (435) Ella

Observed previously by Barucci et al. (1992) and Piironen et al. (1998), Ella showed rather regular lightcurves with periods of 4.623 h and 4.624 h, respectively.

Our observations confirmed this behaviour and synodic period values (Figs. 51–56). Interesting features can be noticed in the shape of the minima. The amplitudes did not change much between the apparitions, always reaching 0.4–0.5 mag.

Although all of the seven apparitions were unevenly distributed along Ella's orbit and clumped into groups, a unique spin and shape model was easily found using 18 lightcurves (see Table 3 for the model parameters). The resulting shape model and lightcurve fits can be found in Figs. 12 and 11.

3.7. (505) Cava

Photometric observations of Cava started in 1975 with the work of Lagerkvist et al. (1978) and continued in Harris & Young (1980), Young & Harris (1985), Harris et al. (1999), and Chiorny et al. (2003, 2007). Most of these papers agreed in the synodic period value being close to 8.178 h.

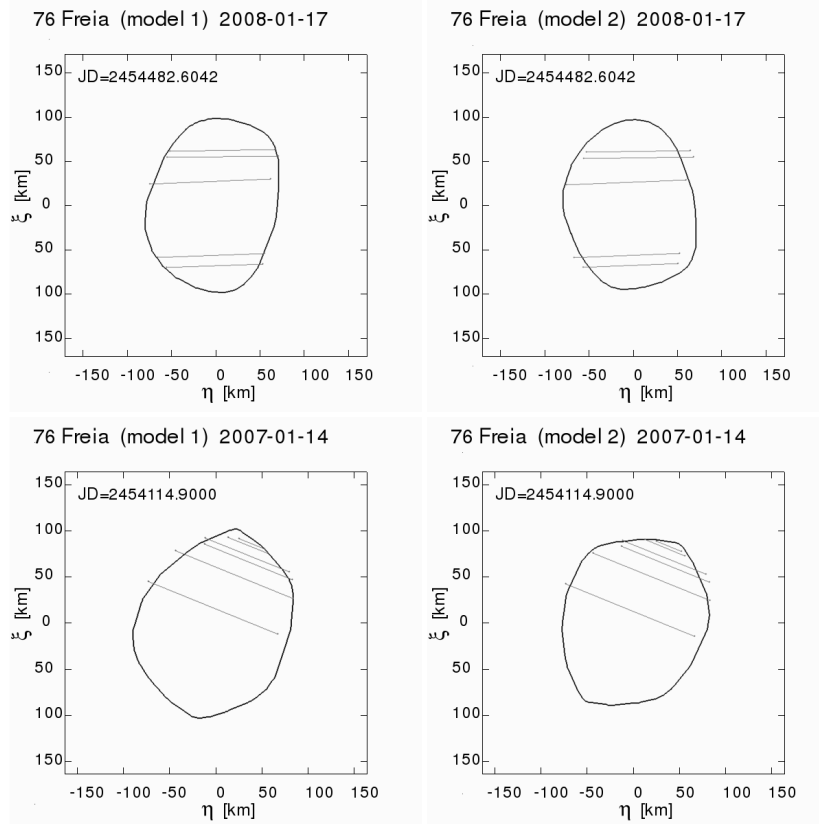


Fig. 17. Occultation chords with both scaled shape models for asteroid (76) Freia. Two occultation events.

We observed this asteroid during five apparitions, starting in 1997. Our data confirmed the period value and the irregularity of the lightcurve shapes (see Figs. 57–61 for composite lightcurves). It displayed amplitudes in the range of 0.13–0.28 mag. In the apparition at the turn of 2004 and 2005, the phase angle (α) span was especially large, reaching an unprecedented 29°. Such data are good indicators of the shadowing properties of the surface and of great value in shape modelling.

During our modelling, we found three short but noisy lightcurves, which prevented us from finding a best-fit solution. After excluding them, a final dataset contained 40 lightcurves from 8 apparitions (counting both our and literature data), and a unique spin and shape model was found (see Table 3). Our model is similar to the one found by Michałowski (1996), even though only in the pole longitude values, but disagrees with the early model of Young & Harris (1985). The shape model visualisations and example lightcurve fits are given in Figs. 14 and 13.

3.8. (699) Hela

The first lightcurve studies of this asteroid were those of started by Pilcher (1983) and Binzel (1987). Subsequent data were gathered by Harris & Young (1999), Pilcher et al. (2000), and Szabo et al. (2001). These authors determined its rotational period at different values, for example 3.396 h given by Pilcher (2000).

Data gathered by us spanned six apparitions (Figs. 62–67). Hela exhibited minima of different depths and strongly variable amplitudes (from 0.15 mag to 0.5 mag). The synodic period that fitted all the composite lightcurves was 3.3961 h.

The model with parameters displayed in Table 3 was the only plausible one, though in some of the lightcurves the fit was unsatisfactory (Fig. 15) and the shape model vertical dimension

(Fig. 16) was poorly constrained, because most of the possible shape models were unnaturally flat. Models with more extrema per period were checked, but were found to be implausible. This model was based on 21 lightcurves from 7 apparitions.

4. Comparison with occultation chords

We implemented the method described by ďurech et al. (2011) to compare newly created photometric models with available data on stellar occultations by these asteroids. Only three of the asteroids modelled here had occultation data with a sufficient number of chords. Comparison of the photometric models with occultation chords provides invaluable information in at least two ways: it gives a confirmation of the shape models, sometimes allowing for the rejection of the mirror pole solution, and the comparison also gives an independent size determination.

In Figs. 17–19, silhouettes were produced when the shape models' orientations were displayed for the given moment of occultation, and were overlayed on the occultation chords (timing data came from the pds (Planetary Data System) occultation database, Dunham et al. 2011). The models were scaled to minimise the χ^2 measure from the occultation chords. The frame in the figures is scaled in km on the Earth fundamental plane (ξ , η) defined in ďurech et al. (2011). Unfortunately, in these specific cases, none of the mirror models can be rejected with certainty. We applied no mutual shifting to the visually acquired chords, because there were not enough electronically measured chords for reference. Nevertheless, the main outlines of the model shapes are confirmed. The sizes of the equivalent volume spheres, with $1-\sigma$ standard deviation, are given in Table 4, where they are compared to the IRAS (Tedesco et al. 2004) and AKARI infrared results (Usui et al. 2011). Our results

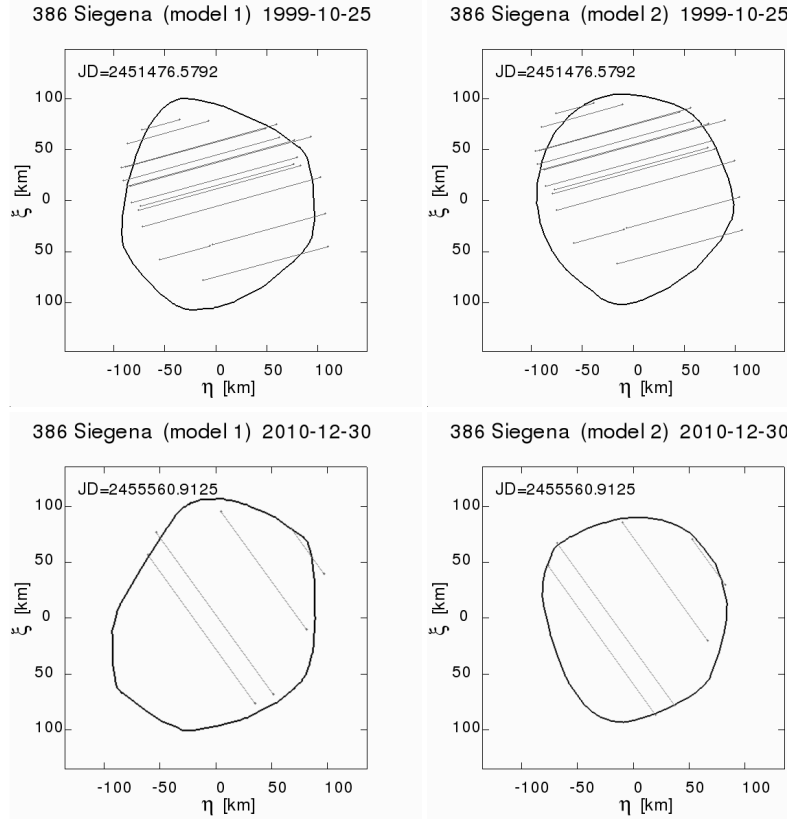


Fig. 18. Occultation chords with both scaled shape models for asteroid (386) Siegena. Two occultation events.

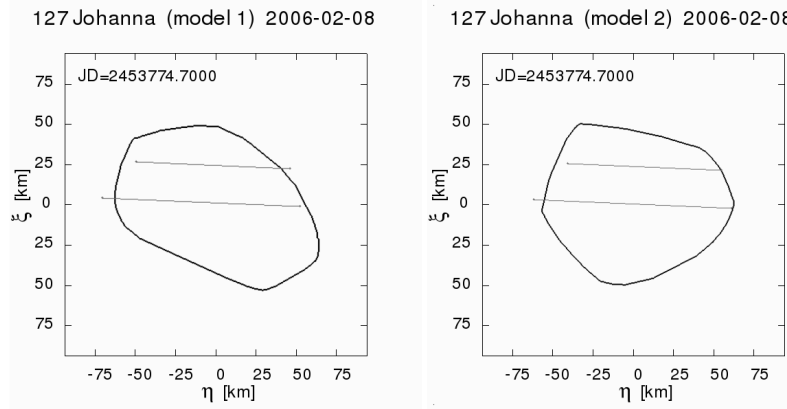


Fig. 19. Occultation chords with both scaled shape models for asteroid (127) Johanna.

are consistent with these sources within the error values. In the case of (76) Freia, our results are closer to AKARI measurements than to previously available IRAS data (Tedesco et al. 2004), while for (386) Siegena our value is exactly between the two. The diameters derived from stellar occultation data are less model-dependent than from other techniques (such as the instantaneous infrared flux observations), provided there is more than one event observed. In that case, the derived diameters do not depend strongly on the momentary model orientation at the time of occultation, because we register the asteroid's shape cross-section in more than one rotational phase. It would even be possible to incorporate the occultation data into the modelling process itself, thus more tightly constraining the resulting spin and shape parameters. However, in these particular cases, both the quality of the available data and a posteriori

Table 4. Equivalent sphere diameters based on fitting to occultation chords (D), compared to their IRAS (D_{IRAS}) and AKARI (D_{AKARI}) values.

Asteroid	D [km]	D_{IRAS} [km]	D_{AKARI} [km]
(76) Freia, Pole 1	169 ± 18	184 ± 4	168 ± 2
Pole 2	165 ± 19		
(127) Johanna, Pole 1	116 ± 14	–	114.2 ± 1.5
Pole 2	108 ± 10		
(386) Siegena, Pole 1	183 ± 22	165 ± 3	201.2 ± 3.5
Pole 2	178 ± 18		

fits are imperfect, so our diameter estimates can only be treated as approximate.

5. Interactive service for asteroid models (ISAM)

The field of asteroid modelling from disk-integrated photometry has started to draw on research advances in the previously separate fields of adaptive optics imaging, observations made at infrared wavelengths, or stellar occultations. There is now quite a large number of asteroids for which it is possible to cross-check or modify models based on photometric data using models from different techniques. However, a common tool was needed to allow for a comparison of both models in the plane of sky at a given epoch.

We thus created an interactive service where this can be done. On the ISAM webpage⁸, one can choose a polyhedral asteroid model and display its orientation for any requested date and in different modes, including stereoscopic views. One can also generate animations, both for the rotating model and the resulting lightcurve. Making predictions for the future light variations and object orientations is also possible. Our orientating codes were cross-checked against adaptive optics (Marciniak et al. 2011) and occultation observations (George et al. 2011). All of the model snapshots shown next to the composite lightcurves (Figs. 21–67, see Appendix) were created with this service.

5.1. Service description

The transformations necessary to fit the data from other techniques utilise the asteroid model with its spin axis defined in an ecliptic coordinate frame, to perform a sky-plane projection where the celestial north is up and east is left, as in the conventional displays of either occultation results or adaptive optics images.

We start from the body model defined by triangular facets in its own reference frame, with the “z” axis coinciding with the axis of rotation and the “x” axis usually orientated according to the epoch of its first photometric observation. We then apply a series of rotations to the model using the orientating algorithm, which first rotates the body by three angles defined by the model’s spin axis ecliptic coordinates and a rotation angle at a specific epoch. The algorithm then takes into account the target’s position with respect to the Earth and the Sun, resulting from its orbital parameters, and projects the body onto the plane perpendicular to the observer-asteroid vector. Finally, this 2D image is rotated so that north is at the top and east is to the left.

The service was developed in LAMP (Linux, Apache, MySQL, PHP) technology and works on a Debian GNU/Linux 6.0 operating system. The management of the www sites is done with Apache ver.2, while the site is based on the PHP 5.0 language and HTML forms with the addition of JavaScript. The PHP code works with the programmes written in C++ language. The C++ codes use the “z-buffer” algorithm to plot the asteroid orientation and return “png” type images. In both modifying the images and creating animations and the three-dimensional (3D) effects, the functions “convert” and “composite” from the Image Magick package are used. Data on the asteroid models and their orbital parameters are stored in the MySQL database. This approach allows for an efficient application run. In the near future, the applications will be installed on the computer cluster and managed with the CORBA (Common Object Request Broker Architecture) and CUDA (Compute Unified Device Architecture) technologies, using GPU.

5.2. Model

In the “model” mode of the ISAM service, one can see the basic, equatorial view of the model. The viewing and lighting geometries can be changed here by selecting different ellipsoidal coordinates of an observer and the Sun over an asteroid’s surface, with an adjustable step. The coordinate system is similar to a geographic longitude λ and latitude ϕ , which here are an astero-centric longitude L and latitude B . If the model is nonconvex, as in the case of (25 143) Itokawa from Hayabusa spacecraft, the shadowing effects can clearly be seen. A 3D stereoscopic view, in the form of an anaglyph, can also be generated here and observed with the usage of special colour glasses.

5.3. Orientation

A short description is provided at the webpage of how to use the “orientation” mode. This is the place where one can generate the model plane-of-sky views for any requested date and time (restricted to the calendar years 1700–3000). Both Julian and Gregorian date formats are possible. A display of a legend can be adjusted and additional options can be chosen. If parameters remain unchanged, the model orientation for the present moment is displayed. To generate the lightcurve that the model would produce at a given orientation, one needs to choose the “Generate lightcurve” option. The plotted lightcurve takes a few seconds to be generated and can be downloaded, both as a plot or in the form of data file.

In Fig. 20, the outcome of the “orientation” mode is shown. The displayed model is described by the Julian date, coordinates of the north pole, an aspect angle, and the period of rotation bound to a specific model solution. The north and east directions in the plane-of-sky are also shown. Images with their legends can be displayed in black and white and downloaded for the use in publication, provided that a proper reference is given.

One of the novelties of the displaying tool is the visibility of the rotation axis, which is marked by a straight line piercing the poles and has a length that depends on the viewing angle. To help one visualise the axis in space, a small circle is shown over the north pole, which changes its shape with changing viewing angle. It also shows the sense of rotation and moves when the animation mode is used.

For research purposes, views corrected for light-travel time are possible. Choosing this option does not affect the JD epoch, but changes the model orientation to the rotation phase later compared to the default one (seen from the Earth). For some applications, e.g., the occultation observations, the full silhouette of the shape model can be displayed. Normally, only the visible and illuminated parts of the model are shown against a black background (as in our example in Fig. 20). Three different 3D effect options are also possible, provided that the lightcurve is not requested. These are an anaglyph, cross-eye, and parallel views. They allow for a spatial view of a model.

5.4. Video

The “video” mode is probably the most interesting for illustrative purposes. It allows one to create an animated model rotation, with the addition of a lightcurve generated live. Possible options in this mode are similar to those in the “orientation” mode, with the addition of an adjustable number of frames per period. The movie takes a few minutes to be fully generated, but the intermediate stages are displayed. For detailed analysis, we recommend generating a slower running movie by choosing more frames per

⁸ <http://isam.astro.amu.edu.pl>

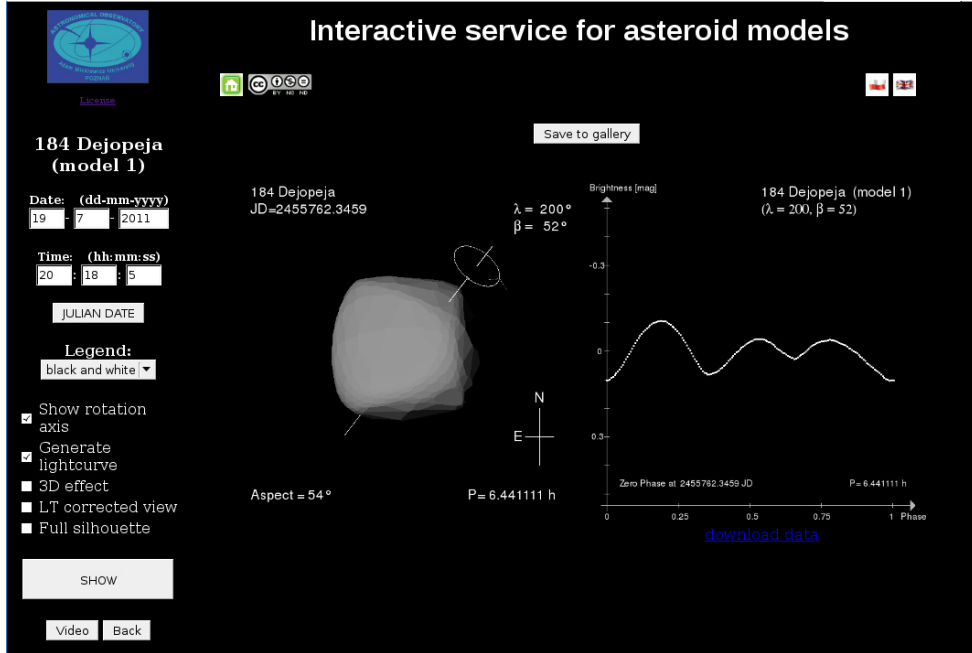


Fig. 20. Example view of the “orientation” mode of the ISAM service. One of our earlier models is displayed.

period. The date typed in the “orientation” mode and the chosen options are transferred here, to allow for an investigation of how various lightcurve features are created by a rotating model.

Any generated views or movies can be saved to the gallery by a user. The galleries are divided into four categories: movie, picture, lightcurve, and plot gallery. The static and animated model views created by other users can be viewed here, where images in the picture and plot galleries are static, while in the movie and lightcurve galleries they are animated.

6. Summary and future plans

The eight models obtained in this work have enlarged the statistical sample of asteroid spin and shape models, partly in an attempt to overcome the observational bias against long periods and low pole latitudes. In three cases, we obtained their size values by comparing with stellar occultation chords, which are independent of both absolute magnitudes and albedo determinations.

Our ISAM web-based service was created to allow a visual comparison of shape models with occultations and for a variety of other applications. It has been designed to aid both researchers and tutors in the community studying asteroids. It allows the direct comparison of photometric asteroid models to those obtained with different techniques, and can be used without any limitations to conduct further research. After the service upgrade, it will be possible to directly derive the model absolute dimensions from the comparison with occultation data. Moreover, as the tool will provide a monochromatic flux for a model’s temporary cross-section, it will be possible to recalibrate asteroid diameter determinations based on infrared data gathered by satellites in the past.

In the near future, we plan to move the service to a computer cluster, which will improve its functionality. The models in the database, which are now mostly from the DAMIT database, can come from various sources and techniques, and we plan to include models based on, e.g., radar ranging or space probe imaging (such as already available model of (25 143) Itokawa).

We also plan to add an option to allow users to temporarily upload their own models and check both their lightcurves and/or orientations.

Acknowledgements. We thank Josef Ďurech for useful comments that led to substantial improvement of our service. This work was supported by grant N N203 404139 from the Polish Ministry of Science and Higher Education. The work of TSR was carried out through the Gaia Research for European Astronomy Training (GREAT-ITN) network. He received funding from the European Union Seventh Framework Programme (FP7/2007–2013) under grant agreement No. 264895. This work is partially based on observations made at the South African Astronomical Observatory (SAAO). Part of the data presented here were taken during a summer school organised by the Niels Bohr Institute at the Nordic Optical Telescope in 2008. We use the convex version of the *lightcurve inversion* code, designed by M. Kaasalainen and modified by J. Ďurech, which is available at <http://astro.troja.mff.cuni.cz/projects/asteroids3D>.

References

- Armstrong, J. C., Nellermoe, B. L., & Reitzler, L. E. 1996, I.A.P.P.P. Comm., 63, 59
- Barucci, M. A., Di Martino, M., & Fulchignoni, M. 1992, AJ, 103, 1679
- Berthier, J., Hestroffer, D., Carry, B., et al. 2008, Asteroids, Comets, Meteors 2008 held July 14–18, in Baltimore, Maryland, LPI Contribution No. 1405, id. 8374
- Binzel, R. P. 1987, Icarus, 72, 135
- Blanco, C., & Riccioli, D. 1998, A&AS, 131, 385
- Bus, S. J., & Binzel, R. P. 2002, Icarus, 158, 146
- Chiorny, V. G., Shevchenko, V. G., Krugly, Yu. N., Velichko, F. P., & Gaftonyuk, N. M. 2003, in Abstracts of Photometry and Polarimetry of Asteroids: Impact on Collaboration, Kharkiv, 9
- Chiorny, V. G., Shevchenko, V. G., Krugly, Yu. N., Velichko, F. P., & Gaftonyuk, N. M. 2007, Planet. Space Sci., 55, 986
- Di Martino, M., Dotto, E., Barucci, M. A., Fulchignoni, M., & Rotundi, A. 1994, Icarus, 109, 210
- Dunham, D., Herald, D., Frappa, et al. 2011, Asteroid Occultations V9.0. EAR-A-3-RDR-OCCULTATIONS-V9.0, NASA Planetary Data System, 2011
- Ďurech, J. 2006, IAU 2006, poster paper
- Ďurech, J., Kaasalainen, M., Warner, B. D., et al. 2009, A&A, 493, 291
- Ďurech, J., Sidorin, V., & Kaasalainen, M. 2010, A&A, 465, 331
- Ďurech, J., Kaasalainen, M., Herald, D., et al. 2011, Icarus, 214, 652
- George, T., Timerson, B., Beard, T., et al. 2011, J. Double Star Obs., 7, 175
- Hanuš, J., Ďurech, J., Brož, M., et al. 2011, A&A, 530, A134
- Harris, A. W., & Young, J. W. 1980, Icarus, 43, 20

- Harris, A. W., & Young, J. W. 1983, *Icarus*, 54, 59
- Harris, A. W., Young, J. W., Dockweiler, T., et al. 1992, *Icarus*, 95, 115
- Harris, A. W., Young, J. W., Bowell, E., & Tholen, D. J. 1999, *Icarus*, 142, 173
- Kaasalainen, M., & Torppa, J. 2001, *Icarus*, 153, 24
- Kaasalainen, M., Torppa, J., & Muinonen, K. 2001, *Icarus*, 153, 37
- Kryszczyńska, A., Colas, F., Berthier, J., Michałowski, T., & Pych, W. 1996, *Icarus*, 124, 134
- Lagerkvist, C.-I. 1978, *A&AS*, 31, 361
- Lagerkvist, C.-I., Hahn, G., Magnusson, P., Rickman, H., & Hammarback, G. 1986, in *Asteroids, Comets, Meteors II*, eds. C.-I. Lagerkvist, B. A. Lindblad, M. Lundstedt, & H. Rickman, Uppsala, 67
- Lagerkvist, C.-I., Hahn, G., Magnusson, P., & Rickman, H. 1987, *A&AS*, 70, 21
- Marchis, F., Kaasalainen, M., Hom, E. F. Y., et al. 2006, *Icarus*, 185, 39
- Marciniak, A., Michałowski, T., Polińska, M., et al. 2011, *A&A*, 529, A107
- Michałowski, T. 1996, *Icarus*, 123, 456
- Michałowski, T., Kwiatkowski, T., Kaasalainen, M., et al. 2004, *A&A*, 416, 353
- Piironen, J., Lagerkvist, C.-I., Erikson, A., et al. 1998, *A&AS*, 128, 525
- Pilcher, F. 1983, *Minor Planet Bull.*, 10, 18
- Pilcher, F., Warner, B. D., & Goretti, V. 2000, *Minor Planet Bull.*, 27, 56
- Shevchenko, V. G., Chiorny, V. G., Gaftonyuk, N. M., et al. 2005, *Abstr. IAU Symp.*, 229, 133
- Shevchenko, V. G., Chiorny, V. G., Gaftonyuk, M., et al. 2008, *Icarus*, 196, 601
- Stephens, R. D. 2005, *Minor Planet Bull.*, 32, 2
- Stephens, R. D. 2007, *Minor Planet Bull.*, 34, 64
- Stephens, R. D., & Warner, B. D. 2008, *Minor Planet Bull.*, 35, 84
- Szabó, Gy. M., Csak, B., Sarnecký, K., & Kiss, L. L. 2001, *A&A*, 375, 285
- Tedesco, E. F., Noah, P. V., Noah, M., & Price, S. D. 2004, *IRAS Minor Planet Survey, IRAS-A-FPA-3-RDR-IMPS-V6.0*, NASA Planetary Data System, 2004
- Timerson, B., Ďurech, J., Aguirre, S., et al. 2009, *Minor Planet Bull.*, 36, 98
- Toth, I. 1997, *Planet. Space Sci.*, 45, 1625
- Usui, F., Kuroda, D., Mueller, T., et al. 2011, *Pub. Astron. Soc. Japan*, 63, 1117
- Warner, B. D., Harris, A. W., & Pravec, P. 2009, *Icarus*, 202, 134
- Young, J., & Harris, A. W. 1985, *Icarus*, 64, 528
- Zappala, V., Scaltriti, F., Lagerkvist, C.-I., Rickman, H., & Harris, A. W. 1982, *Icarus*, 52, 196

Appendix: Lightcurve data

Table 1. Aspect data.

Date (UT)	r (AU)	Δ (AU)	Phase angle (°)	λ (J2000) (°)	β (°)	N_p	σ	Obs.
								(mag)
(76) Freia								
2002-02-28.9	2.9174	2.1072	13.20	117.98	-2.81	38	0.010	Bor
2002-03-10.9	2.9258	2.2135	15.63	117.63	-2.64	55	0.010	Bor
2002-04-01.9	2.9461	2.4955	18.93	118.90	-2.30	37	0.005	Bor
2002-04-02.8	2.9471	2.5091	19.02	119.02	-2.28	18	0.017	Bor
2002-04-05.9	2.9500	2.5512	19.25	119.41	-2.23	24	0.008	Bor
2002-04-08.8	2.9530	2.5931	19.44	119.83	-2.19	25	0.018	Bor
2006-09-15.9	3.3849	2.4001	4.09	6.76	1.12	51	0.006	Bor
2006-09-21.0	3.3772	2.3800	2.40	5.85	1.08	80	0.008	Bor
2006-10-09.8	3.3482	2.3708	4.16	2.32	0.93	51	0.011	Bor
2007-10-08.0	2.8946	2.5594	19.92	95.00	-1.84	13	0.004	Bor
2007-10-14.0	2.8910	2.4767	19.53	95.90	-1.94	22	0.002	Bor
2007-10-15.1	2.8903	2.4621	19.44	96.05	-1.96	25	0.006	Bor
2008-01-03.9	2.8620	1.8963	4.55	89.74	-2.99	56	0.029	Bor
2008-01-12.0	2.8612	1.9301	7.71	88.32	-2.97	67	0.003	Bor
2008-01-14.0	2.8611	1.9408	8.43	88.02	-2.96	107	0.009	Bor
2009-04-15.9	3.3126	2.3864	7.87	179.17	-0.89	58	0.008	Bor
2009-04-24.9	3.3264	2.4655	10.42	178.08	-0.79	43	0.009	Bor
2009-04-28.9	3.3326	2.5065	11.43	177.72	-0.75	42	0.012	Bor
2009-05-13.9	3.3556	2.6864	14.48	177.08	-0.60	29	0.008	Bor
2010-04-25.0	3.8110	2.9308	8.36	248.09	1.58	136	0.004	SAAO
2010-04-26.9	3.8128	2.9173	7.90	247.86	1.60	33	0.016	SAAO
(127) Johanna								
2000-10-28.8	2.7659	1.7911	4.91	21.95	-1.06	38	0.030	ChR
2002-01-11.2	2.5776	1.6934	11.84	141.01	12.48	50	0.030	ChR
2002-01-12.1	2.5777	1.6876	11.52	140.88	12.51	82	0.040	ChR
2005-11-08.8	2.6574	1.7390	9.91	73.21	6.72	16	0.013	Bor
2005-11-13.1	2.6550	1.7146	8.29	72.47	7.00	54	0.029	Bor
2005-12-01.8	2.6447	1.6649	3.01	68.38	7.99	39	0.010	Bor
2005-12-29.9	2.6302	1.7727	12.80	62.88	8.54	51	0.007	Bor
2006-01-07.9	2.6259	1.8458	15.62	62.03	8.49	93	0.007	Bor
2006-01-15.9	2.6222	1.9234	17.73	61.75	8.39	84	0.010	Bor
2007-02-04.0	2.6355	1.9639	18.25	191.41	6.91	31	0.011	Bor
2007-03-17.9	2.6581	1.6753	4.25	186.42	6.32	31	0.007	Bor
2007-03-25.0	2.6622	1.6686	2.28	184.81	6.02	83	0.007	Bor
2007-03-29.0	2.6645	1.6711	2.63	183.91	5.83	87	0.011	Bor
2007-04-06.0	2.6693	1.6893	5.43	182.14	5.40	74	0.024	Bla
2007-04-07.0	2.6699	1.6929	5.84	181.93	5.34	90	0.013	Bla
2007-04-18.0	2.6765	1.7483	10.14	179.91	4.68	100	0.013	Bla
2007-04-22.9	2.6795	1.7824	11.91	179.20	4.37	23	0.012	Bor
2007-05-07.9	2.6889	1.9178	16.48	177.97	3.42	50	0.024	Bla
2007-05-09.0	2.6895	1.9284	16.73	177.94	3.36	45	0.017	Bla
2007-05-09.9	2.6901	1.9384	16.96	177.92	3.30	45	0.019	Bla
2007-05-10.9	2.6907	1.9493	17.21	177.90	3.24	44	0.018	Bla
2007-05-12.9	2.6920	1.9709	17.66	177.89	3.12	73	0.016	Bla
2008-06-06.0	2.9108	2.0011	10.70	286.11	-10.85	136	0.007	SAAO
2008-06-06.2	2.9109	2.0000	10.65	286.09	-10.86	50	0.007	SAAO
2008-06-14.8	2.9135	1.9528	7.94	284.65	-11.28	57	0.024	SAAO
2009-08-09.1	2.8552	2.2154	18.00	16.93	-5.73	87	0.008	SAAO
2009-09-20.0	2.8316	1.8540	5.77	12.83	-5.16	91	0.009	Bor
2009-11-05.9	2.8028	1.9689	13.09	3.81	-2.95	71	0.012	Bor
2009-12-02.8	2.7854	2.2529	19.06	3.40	-1.58	61	0.018	Bor
2011-02-09.0	2.5762	1.6746	11.06	112.41	12.74	27	0.007	Bor
2011-03-04.9	2.5761	1.8693	18.23	110.40	11.30	144	0.010	Bor
2011-03-08.9	2.5762	1.9107	19.10	110.46	11.03	92	0.004	Bor
(355) Gabriella								
2005-12-23.0	2.2779	1.3238	7.88	74.16	7.38	79	0.011	Cre
2005-12-23.9	2.2777	1.3269	8.31	73.97	7.36	52	0.010	Cre
2006-01-16.8	2.2723	1.4760	18.14	70.89	6.55	58	0.011	Bor
2006-01-28.7	2.2709	1.5878	21.53	71.04	6.03	20	0.006	Bor
2007-05-23.8	2.6674	1.7673	12.25	208.62	-4.85	48	0.004	SAAO
2008-08-22.0	2.7440	1.7906	8.73	305.28	-4.06	12	0.031	LaP
2008-08-22.9	2.7434	1.7952	9.08	305.11	-4.03	82	0.004	LaP
2009-09-09.3	2.3570	2.0313	25.16	70.88	4.01	48	0.033	Bor
2009-11-22.0	2.3011	1.3312	6.13	72.33	7.16	89	0.008	Bor
2010-01-22.8	2.2748	1.6079	21.81	63.66	6.06	30	0.006	Bor
2010-01-31.8	2.2728	1.7033	23.57	64.59	5.69	22	0.008	Bor
2010-03-26.8	2.2709	2.3407	24.92	79.64	3.84	32	0.021	Bor

Notes. Mid-date of observation, Sun (r) and Earth (Δ) distance, Sun-asteroid-Earth phase angle, sky position in the ecliptic coordinates (λ, β), number of points per lightcurve (N_p), its quality (σ), and the observatory code. Observatory Code: Bor – Borowiec; ChR – Pic de Château-Renard Observatory; Bla – Blauvac Observatory; SAAO – South African Astronomical Observatory; Cre – Le Crès, France; LaP – La Palma, Canary Islands.

Table 1. continued.

Date (UT)	r	Δ	Phase angle (°)	λ (J2000) (°)	β (°)	N_p	σ (mag)	Obs.
	(AU)	(AU)						
(386) Siegena								
1998-04-16.9	3.3860	2.4230	5.66	194.37	15.13	40	0.015	Bor
1998-04-21.0	3.3869	2.4383	6.61	193.52	15.28	119	0.010	Bor
1998-04-24.0	3.3875	2.4525	7.36	192.93	15.37	111		Bor
1998-05-01.9	3.3891	2.5012	9.38	191.50	15.53	76	0.014	Bor
1999-05-19.0	3.1453	2.3185	12.40	270.11	27.96	23	0.007	Bor
1999-05-20.0	3.1439	2.3105	12.23	269.97	28.05	18	0.003	Bor
1999-05-28.0	3.1327	2.2542	10.91	268.65	28.67	31	0.006	Bor
1999-05-30.0	3.1299	2.2423	10.60	268.28	28.79	27	0.007	Bor
1999-06-05.0	3.1214	2.2123	9.83	267.07	29.09	44	0.007	Bor
2002-02-21.9	2.9834	2.0592	8.14	131.98	-14.34	11	0.007	Bor
2002-04-03.8	3.0499	2.4984	17.38	128.58	-9.17	20	0.008	Bor
2004-06-13.0	3.0648	2.1467	9.71	272.61	28.99	61	0.005	EnO
2007-03-26.9	3.0836	2.3633	14.68	134.73	-8.34	58	0.012	Bor
2007-03-31.9	3.0912	2.4262	15.64	134.55	-7.77	44	0.014	Bor
2007-04-05.9	3.0987	2.4931	16.47	134.52	-7.22	35	0.012	Bor
2007-04-12.9	3.1090	2.5914	17.39	134.72	-6.49	41	0.006	Bor
2008-02-04.2	3.3835	3.0358	16.55	212.34	11.14	14	0.004	Bor
2008-02-17.2	3.3872	2.8593	15.43	212.97	12.52	28	0.003	Bor
2008-03-11.1	3.3917	2.5982	11.56	211.87	15.11	20	0.003	Bor
2008-03-29.0	3.3937	2.4695	7.49	209.12	16.95	48	0.013	Bor
2008-03-30.0	3.3938	2.4647	7.28	208.92	17.04	50	0.005	Bor
2008-04-01.1	3.3939	2.4557	6.84	208.52	17.22	20	0.006	Bor
2008-04-22.0	3.3940	2.4332	5.89	203.96	18.56	16	0.011	Bor
2008-05-10.0	3.3926	2.5110	9.67	200.42	18.89	58	0.003	Bor
2009-04-30.0	3.0864	2.5485	17.47	284.26	24.51	22	0.006	Bor
2009-05-04.0	3.0803	2.4970	17.06	284.42	24.94	38	0.015	Bor
2009-05-19.0	3.0572	2.3238	15.03	284.18	26.49	34	0.008	Bor
2009-08-06.9	2.9249	2.1623	15.27	270.26	24.80	214	0.010	SAAO
2009-08-10.8	2.9182	2.1899	16.02	269.97	24.23	39	0.005	SAAO
2009-08-10.9	2.9180	2.1906	16.04	269.97	24.21	174	0.013	SAAO
2009-08-16.7	2.9078	2.2364	17.09	269.73	23.34	44	0.014	SAAO
2009-08-16.8	2.9076	2.2371	17.10	269.72	23.33	124		SAAO
2009-09-19.8	2.8479	2.5748	20.56	272.49	18.25	17	0.004	Bor
2009-09-26.8	2.8356	2.6522	20.70	273.82	17.29	22	0.006	Bor
2009-09-30.8	2.8285	2.6968	20.70	274.68	16.77	10	0.012	Bor
2010-09-02.1	2.3990	1.7411	21.58	39.38	-14.73	63	0.005	Bor
2010-09-12.0	2.3973	1.6482	19.48	39.77	-16.82	65	0.007	Bor
2010-09-19.1	2.3966	1.5920	17.72	39.61	-18.32	81	0.012	Bor
2010-09-22.1	2.3964	1.5705	16.92	39.42	-18.96	79	0.005	Bor
2010-10-05.1	2.3966	1.4976	13.30	37.84	-21.63	98	0.010	Bor
(417) Suevia								
2001-09-22.9	3.1447	2.2955	11.43	38.27	-1.10	41		Kha
2001-10-14.0	3.1336	2.1568	4.47	34.76	-1.75	55	0.012	Bor
2001-10-24.8	3.1272	2.1333	0.72	32.42	-2.06	27	0.014	Bor
2001-12-13.7	3.0926	2.4413	15.43	25.06	-2.96	10	0.009	Bor
2001-12-21.8	3.0861	2.5386	16.78	25.09	-3.02	40	0.005	Pic
2005-08-30.0	3.1317	2.1321	3.17	344.55	5.98	38	0.014	Bin
2005-08-30.0	3.1317	2.1321	3.17	344.55	5.98	48	0.020	Bla
2005-08-31.0	3.1323	2.1311	2.87	344.34	5.96	58	0.010	Bin
2005-08-31.0	3.1323	2.1311	2.87	344.34	5.96	44	0.019	Bla
2005-09-01.0	3.1328	2.1304	2.59	344.12	5.94	77	0.027	Bla
2005-09-14.0	3.1398	2.1475	3.63	341.34	5.62	35	0.016	Bor
2005-09-21.9	3.1437	2.1812	6.23	339.78	5.36	32	0.020	Bor
2005-09-25.8	3.1456	2.2046	7.53	339.07	5.21	25	0.011	Bor
2005-10-09.8	3.1517	2.3185	11.68	337.12	4.66	46	0.016	Bor
2006-11-19.0	3.0087	2.0238	1.92	55.86	-5.83	58	0.019	Bor
2006-11-30.7	2.9962	2.0367	5.28	53.27	-6.06	13	0.043	Bor
2006-12-08.8	2.9873	2.0685	8.18	51.68	-6.14	32	0.008	Bor
2006-12-11.9	2.9839	2.0854	9.26	51.14	-6.15	137	0.016	Bin
2006-12-13.8	2.9818	2.0967	9.88	50.83	-6.16	36	0.014	Bin
2006-12-21.0	2.9736	2.1481	12.14	49.83	-6.15	115	0.015	Bin
2008-02-04.0	2.4744	1.5874	12.46	166.60	-7.38	67	0.003	Bor
2008-02-14.9	2.4668	1.5177	8.09	164.91	-7.31	35	0.005	Bor
2008-02-15.9	2.4662	1.5128	7.67	164.72	-7.29	36	0.005	Bor
2008-03-30.9	2.4427	1.5550	13.50	156.06	-5.28	49	0.012	Bor
2008-04-01.8	2.4419	1.5679	14.23	155.84	-5.16	12	0.010	Bor
2009-08-08.9	2.8579	1.9829	12.34	280.50	9.55	72	0.005	SAAO
2009-08-09.9	2.8591	1.9921	12.63	280.40	9.50	90	0.012	SAAO
2009-08-14.9	2.8656	2.0407	13.95	279.98	9.29	64	0.004	SAAO
2009-08-15.8	2.8668	2.0508	14.20	279.92	9.24	96	0.015	SAAO
2010-09-11.9	3.1761	2.2117	6.24	8.94	2.79	25	0.006	Bor
2010-09-18.9	3.1768	2.1871	3.77	7.55	2.64	19	0.020	Bor
2010-10-11.9	3.1780	2.2063	4.94	2.67	2.02	36	0.011	Bor
2010-10-26.9	3.1776	2.2993	9.87	0.12	1.56	66	0.014	Bor
2010-12-04.8	3.1728	2.7499	17.33	358.92	0.46	55	0.014	Bor

Notes. Observatory Code: Bor – Borowiec; EnO – Les Engarouines Observatory; SAAO – South African Astronomical Observatory; Kha – Kharkiv, Ukraine Pic – Pic du Midi; Bin – Bedoin, France; Bla – Blauvac Observatory.

Table 1. continued.

Date (UT)	r	Δ	Phase angle (°)	λ (J2000) (°)	β (°)	N_p	σ	Obs.
	(AU)	(AU)					(mag)	
(435) Ella								
2003-01-08.8	2.4000	1.5217	13.28	74.03	2.58	48	0.011	Bor
2003-02-01.7	2.4409	1.7855	20.29	73.22	2.34	19	0.015	Bor
2004-04-22.0	2.8203	1.9615	12.75	173.91	0.75	206	0.040	ChR
2006-12-14.1	2.4546	1.5216	9.33	105.58	2.80	100	0.013	Bla
2006-12-19.0	2.4630	1.5075	7.00	104.47	2.86	132	0.027	Bla
2006-12-22.0	2.4681	1.5021	5.56	103.75	2.88	101	0.022	Bla
2008-04-21.9	2.7922	1.8315	7.50	190.92	0.24	37	0.021	Bor
2008-04-26.9	2.7889	1.8548	9.45	189.94	0.19	46	0.006	Bor
2008-05-06.9	2.7820	1.9194	13.01	188.35	0.09	37	0.007	Bor
2009-08-11.0	2.1312	1.1185	1.51	317.95	-3.15	31	0.007	SAAO
2009-08-14.0	2.1280	1.1172	2.44	317.25	-3.12	236	0.003	SAAO
2009-08-16.9	2.1250	1.1179	3.87	316.59	-3.09	15	0.010	SAAO
2009-08-17.9	2.1240	1.1186	4.38	316.37	-3.07	79	0.024	SAAO
2011-02-21.8	2.6570	1.8219	13.82	112.92	2.58	32	0.007	Bor
2011-03-03.9	2.6700	1.9307	16.72	112.18	2.42	53	0.010	Bor
(505) Cava								
1997-04-02.0	2.7181	1.8159	11.11	163.93	14.69	94	0.015	Bor
2004-10-30.7	2.0966	1.1284	8.18	29.60	-15.60	77		BC
2004-11-03.5	2.0910	1.1306	9.23	28.76	-15.29	126		BC
2004-11-07.5	2.0855	1.1364	10.60	27.95	-14.91	62		BC
2004-11-15.5	2.0748	1.1590	13.82	26.57	-14.00	187		BC
2004-11-16.9	2.0732	1.1642	14.38	26.38	-13.83	130	0.036	Cre
2004-11-18.8	2.0708	1.1723	15.17	26.13	-13.58	82	0.010	Cre
2004-11-25.6	2.0629	1.2060	17.85	25.50	-12.66	50		BC
2004-11-29.8	2.0584	1.2313	19.42	25.32	-12.06	92	0.019	Cre
2004-12-05.8	2.0524	1.2721	21.45	25.32	-11.20	114	0.009	Cre
2005-01-01.8	2.0328	1.5079	27.46	29.15	-7.53	14	0.011	Cre
2005-01-19.9	2.0267	1.6949	28.94	34.52	-5.47	30	0.015	Sab
2006-05-11.9	2.9851	2.2445	15.24	181.23	12.65	27	0.019	Bla
2006-05-15.9	2.9934	2.2948	16.02	181.10	12.36	40	0.008	Bla
2006-05-23.9	3.0095	2.4006	17.31	181.11	11.79	21	0.008	Bla
2006-05-24.9	3.0115	2.4143	17.44	181.13	11.72	35	0.008	Bla
2006-05-27.9	3.0175	2.4568	17.83	181.25	11.50	48	0.008	Bla
2006-05-28.9	3.0195	2.4709	17.94	181.30	11.43	40	0.009	Bla
2006-06-10.9	3.0446	2.6619	19.01	182.40	10.55	11	0.010	Soz
2006-06-13.9	3.0503	2.7076	19.14	182.77	10.35	12	0.035	Bla
2008-06-14.1	2.7956	2.3013	20.15	334.67	-8.26	49	0.005	SAAO
2008-08-22.1	2.6204	1.6265	5.20	329.05	-13.58	12	0.019	LaP
2010-02-28.0	2.4253	1.4816	9.09	140.86	13.67	50	0.006	Bor
2010-03-11.9	2.4568	1.5746	13.34	138.86	13.46	54	0.019	Bor
2010-03-18.9	2.4753	1.6431	15.56	138.14	13.21	43	0.013	Bor
2010-03-30.8	2.5068	1.7788	18.63	137.76	12.67	42	0.012	Bor
2010-04-18.9	2.5574	2.0343	21.66	139.18	11.67	32	0.009	Bor
2010-04-24.9	2.5732	2.1203	22.16	140.06	11.36	59	0.010	Bor
2010-04-30.8	2.5889	2.2076	22.49	141.12	11.06	12	0.012	Bor
2010-05-08.9	2.6101	2.3283	22.67	142.80	10.66	38	0.011	Bor
(699) Hela								
1999-09-05.1	1.5587	0.6447	24.54	353.71	38.48	48	0.007	Bor
1999-09-05.9	1.5594	0.6445	24.39	353.63	38.43	18	0.011	Bor
1999-09-11.0	1.5650	0.6447	23.48	353.11	37.94	116	0.006	Bor
2003-06-29.0	1.9012	0.9439	14.67	250.92	11.69	36	0.023	EnO
2003-06-30.0	1.8968	0.9443	15.26	250.69	11.86	38	0.018	EnO
2003-07-19.0	1.8153	0.9832	25.22	247.95	14.46	79	0.009	Pic
2003-07-21.9	1.8029	0.9937	26.53	247.84	14.77	60	0.020	Pic
2005-02-08.0	3.2390	2.3891	10.32	107.00	-16.99	46	0.020	Pic
2005-02-10.9	3.2473	2.4210	11.04	106.52	-16.89	18	0.006	Pic
2007-05-24.8	2.4498	1.4923	9.89	219.39	-6.15	35	0.004	SAAO
2009-01-06.0	2.8506	1.8981	6.01	94.40	-13.62	44	0.006	Pic
2009-11-27.2	3.6330	3.5595	15.73	158.83	-15.38	34	0.006	Pic
2010-04-18.8	3.6752	3.1544	14.48	143.65	-17.82	34	0.013	SAAO
2010-04-26.8	3.6722	3.2580	15.23	143.68	-17.19	24	0.050	SAAO
2010-05-01.8	3.6701	3.3250	15.57	143.85	-16.81	15	0.005	SAAO

Notes. Observatory Code: Bor – Borowiec; ChR – Pic de Château-Renard Observatory; Bla – Blauvac Observatory; SAAO – South African Astronomical Observatory; BC – Bathurst & Canberra; Cre – Le Crès, France; Sab – Sabadell, Barcelona; Soz – Sozzago, Italy LaP – La Palma, Canary Islands; EnO – Les Engarouines Observatory; Pic – Pic du Midi.

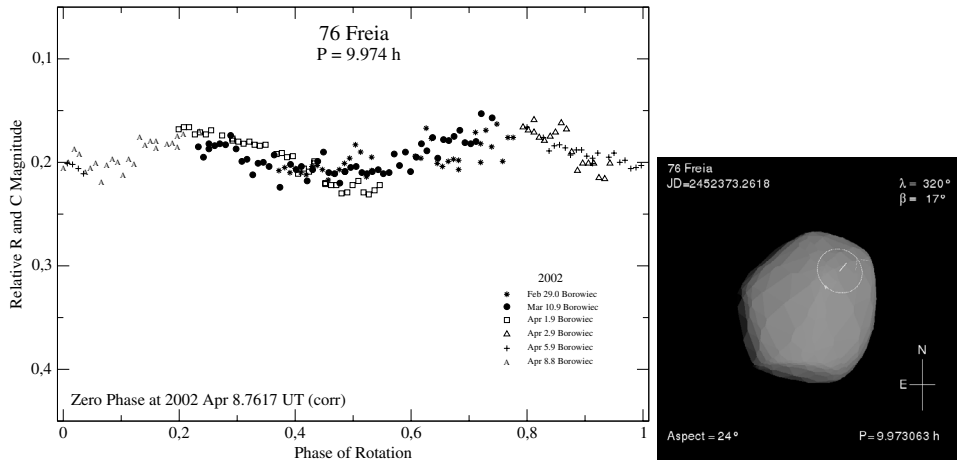


Fig. 21. Composite lightcurve of (76) Freia in 2002 with the orientation of model 2 for the zero phase.

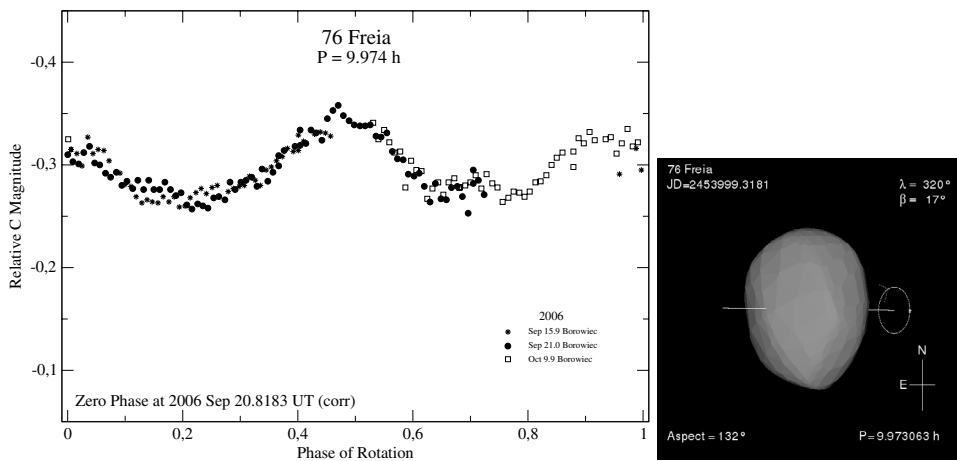


Fig. 22. Composite lightcurve of (76) Freia in 2006 with the orientation of model 2 for the zero phase.

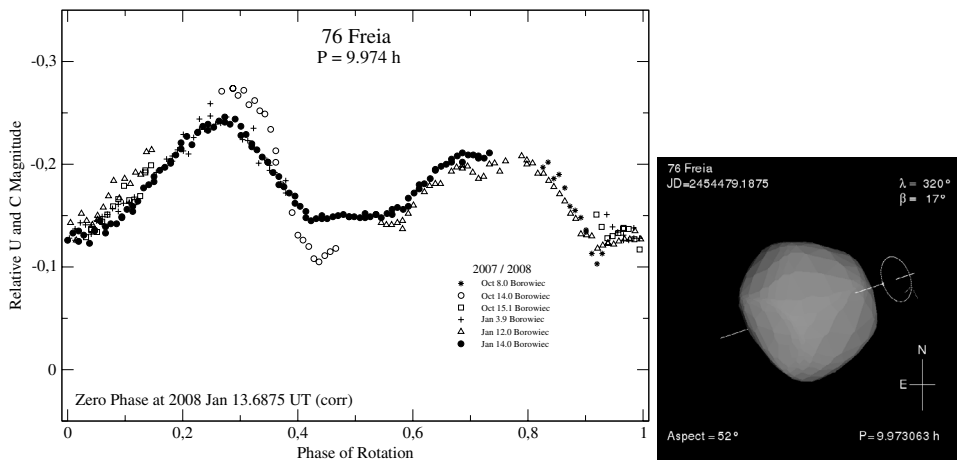


Fig. 23. Composite lightcurve of (76) Freia in 2007/2008 with the orientation of model 2 for the zero phase.

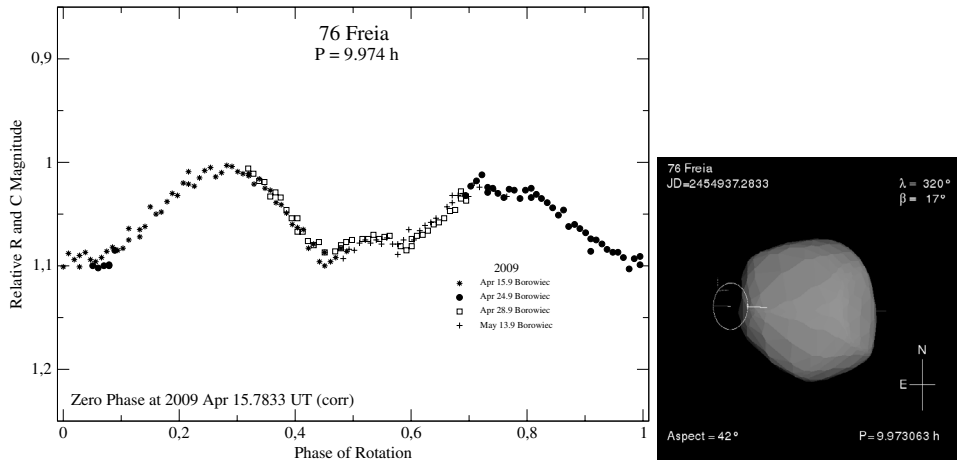


Fig. 24. Composite lightcurve of (76) Freia in 2009 with the orientation of model 2 for the zero phase.

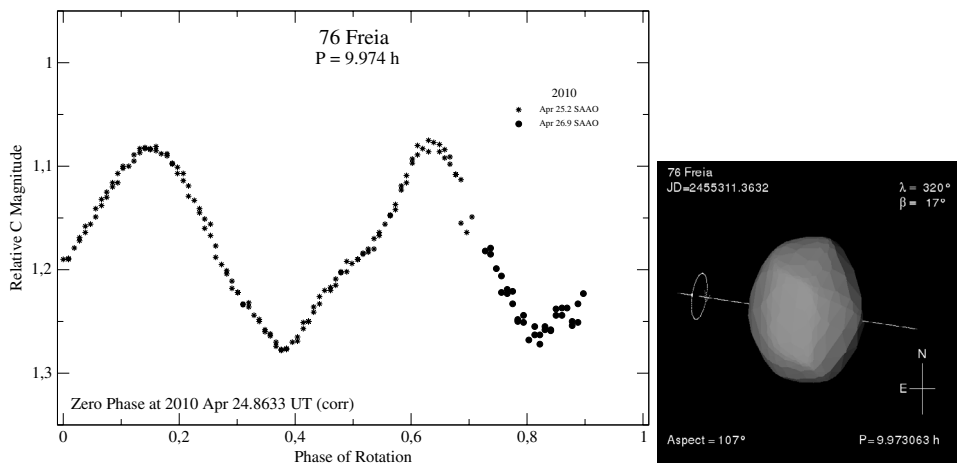


Fig. 25. Composite lightcurve of (76) Freia in 2010 with the orientation of model 2 for the zero phase.

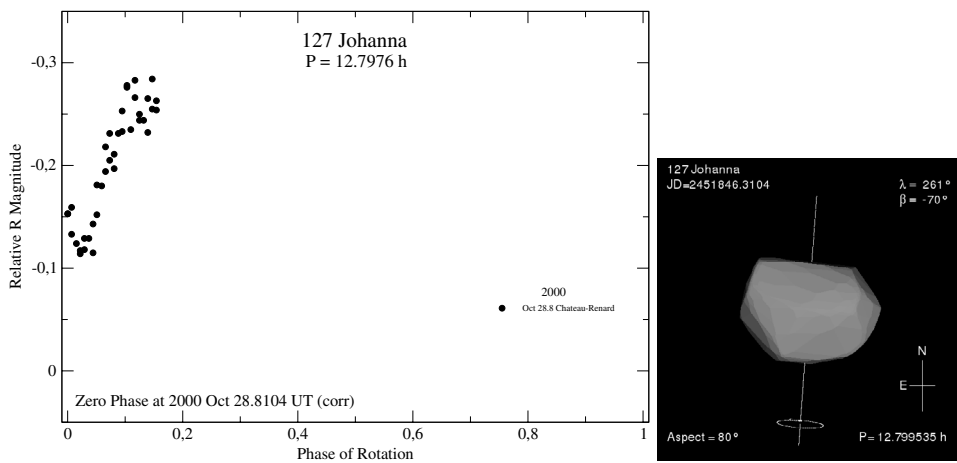


Fig. 26. Composite lightcurve of (127) Johanna in 2000 with the orientation of model 2 for the zero phase.

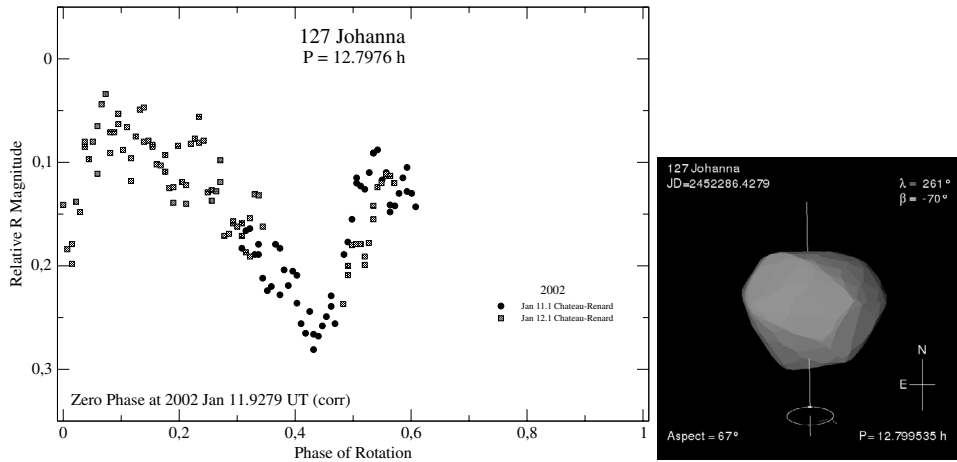


Fig. 27. Composite lightcurve of (127) Johanna in 2002 with the orientation of model 2 for the zero phase.

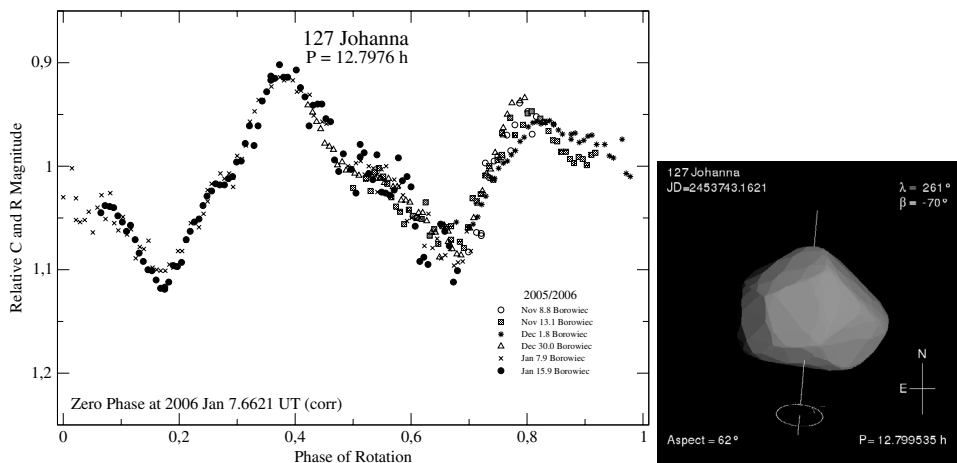


Fig. 28. Composite lightcurve of (127) Johanna in 2005/2006 with the orientation of model 2 for the zero phase.

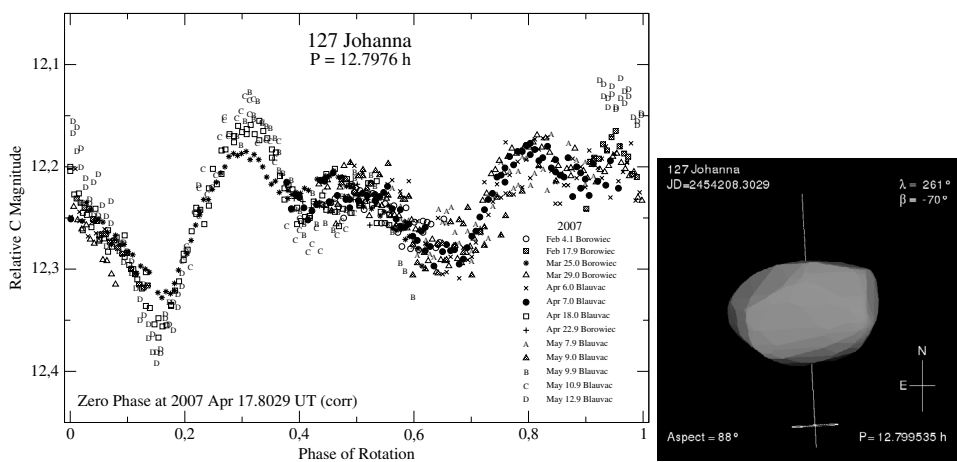


Fig. 29. Composite lightcurve of (127) Johanna in 2007 with the orientation of model 2 for the zero phase.

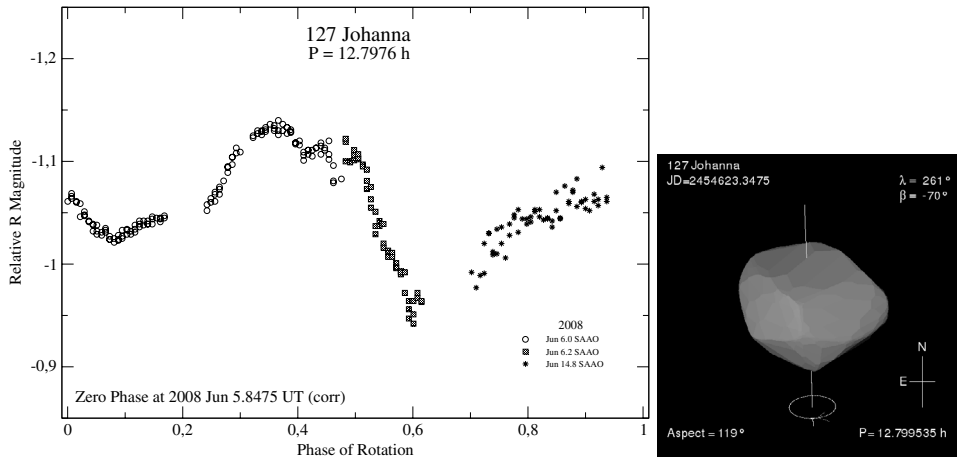


Fig. 30. Composite lightcurve of (127) Johanna in 2008 with the orientation of model 2 for the zero phase.

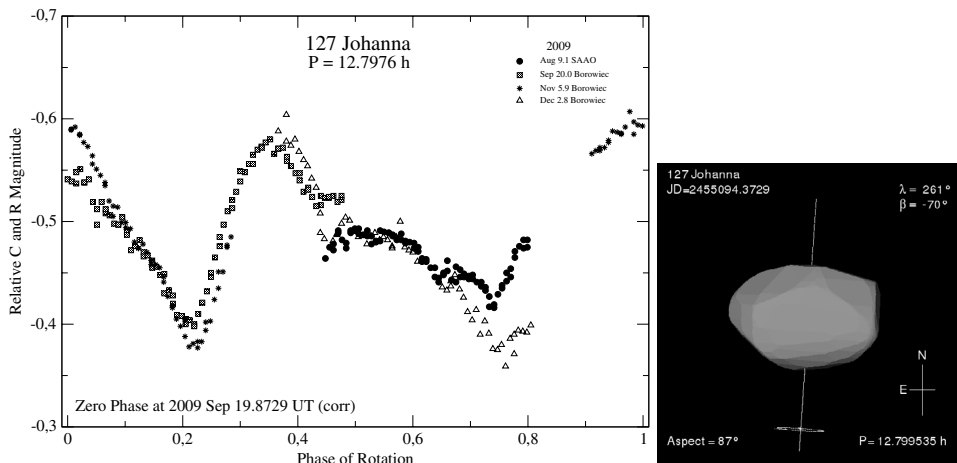


Fig. 31. Composite lightcurve of (127) Johanna in 2009 with the orientation of model 2 for the zero phase.

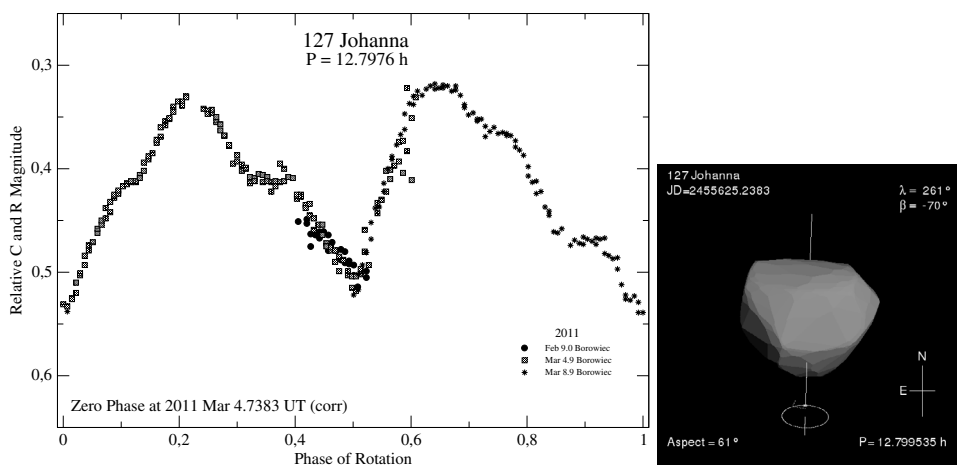


Fig. 32. Composite lightcurve of (127) Johanna in 2011 with the orientation of model 2 for the zero phase.

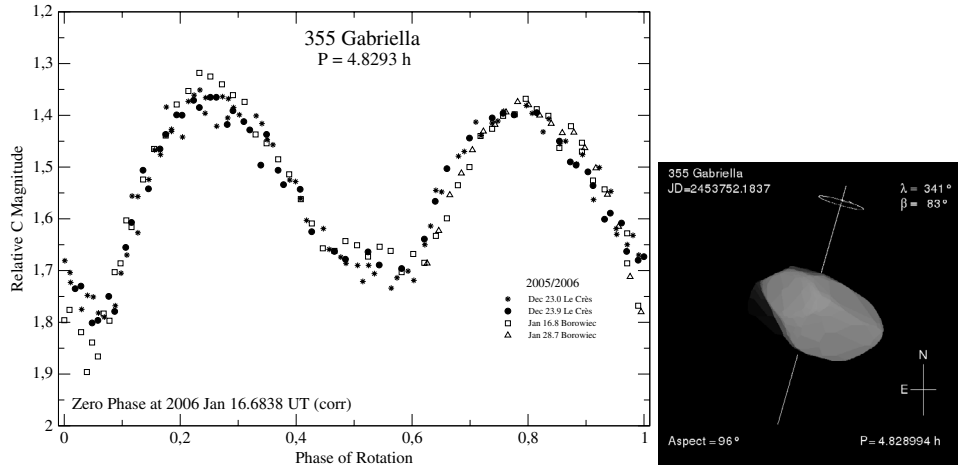


Fig. 33. Composite lightcurve of (355) Gabriella in 2005/2006 with the orientation of model 2 for the zero phase.

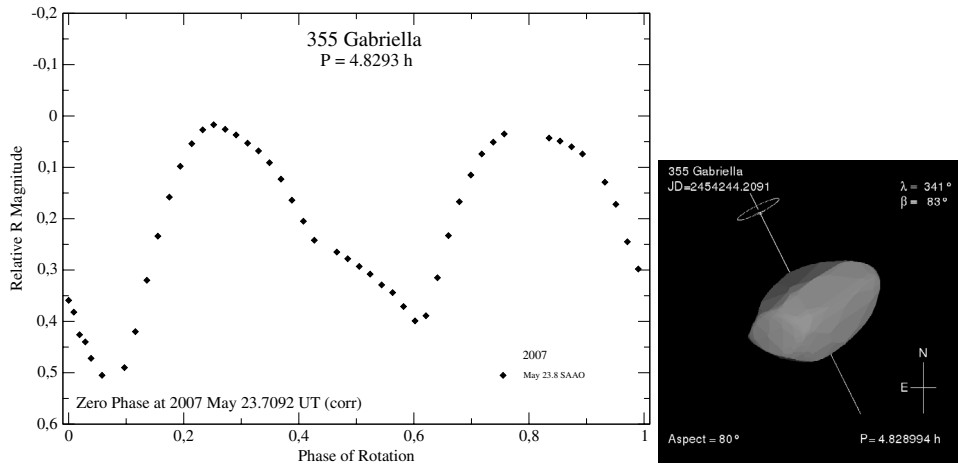


Fig. 34. Composite lightcurve of (355) Gabriella in 2007 with the orientation of model 2 for the zero phase.

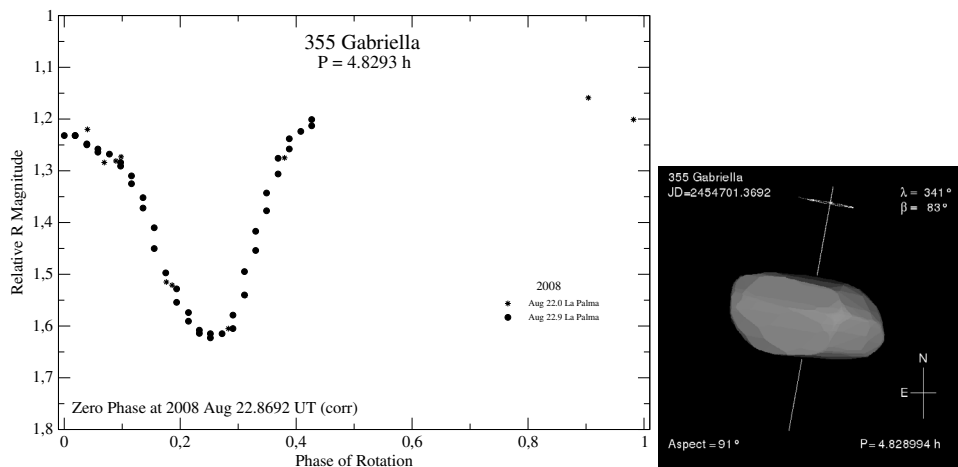


Fig. 35. Composite lightcurve of (355) Gabriella in 2008 with the orientation of model 2 for the zero phase.

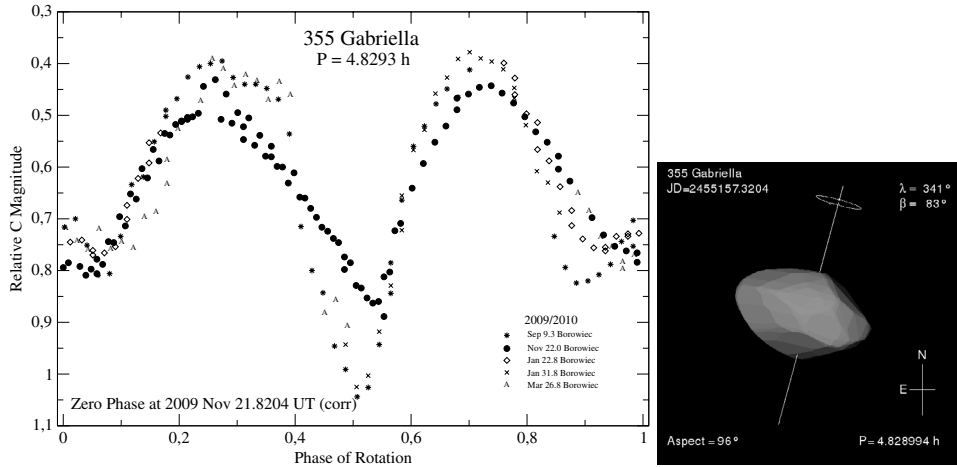


Fig. 36. Composite lightcurve of (355) Gabriella in 2009/2010 with the orientation of model 2 for the zero phase.

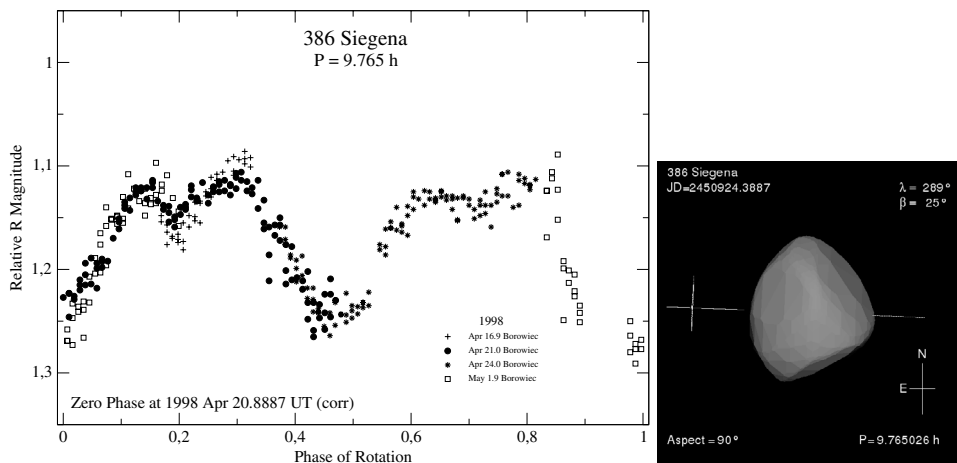


Fig. 37. Composite lightcurve of (386) Siegena in 1998 with the orientation of model 2 for the zero phase.

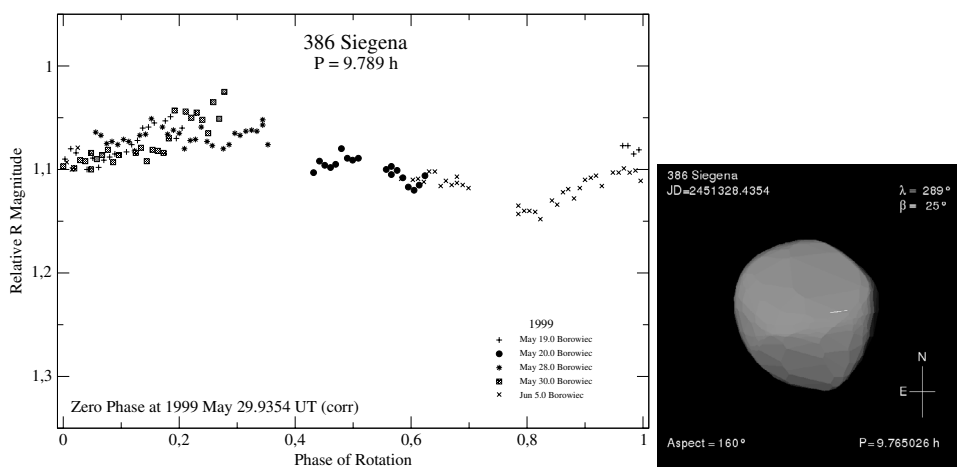


Fig. 38. Composite lightcurve of (386) Siegena in 1999 with the orientation of model 2 for the zero phase.

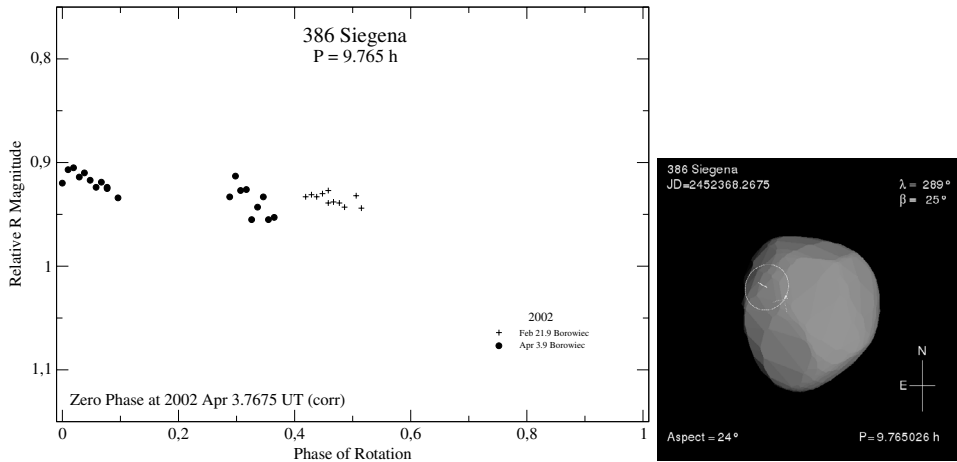


Fig. 39. Composite lightcurve of (386) Siegena in 2002 with the orientation of model 2 for the zero phase.

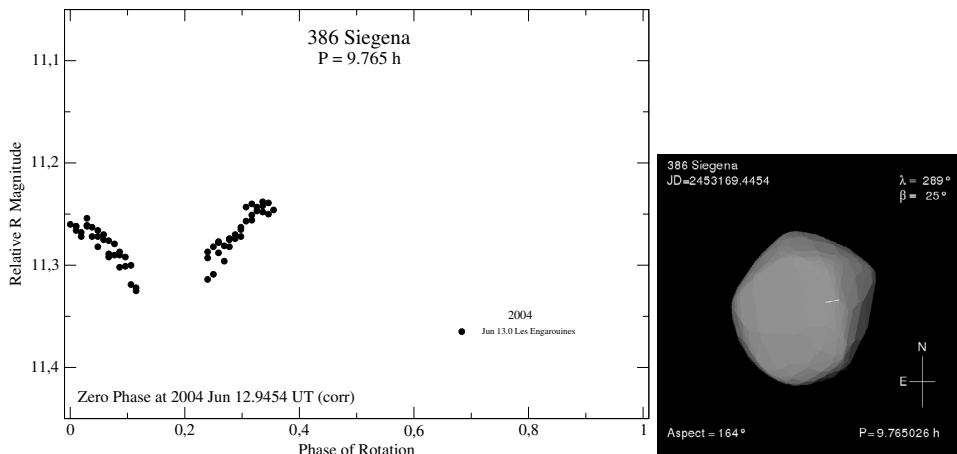


Fig. 40. Composite lightcurve of (386) Siegena in 2004 with the orientation of model 2 for the zero phase.

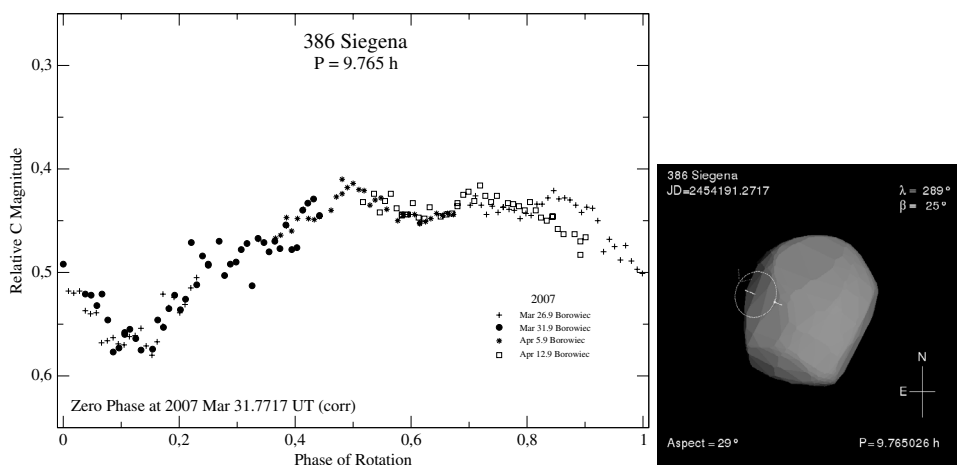


Fig. 41. Composite lightcurve of (386) Siegena in 2007 with the orientation of model 2 for the zero phase.

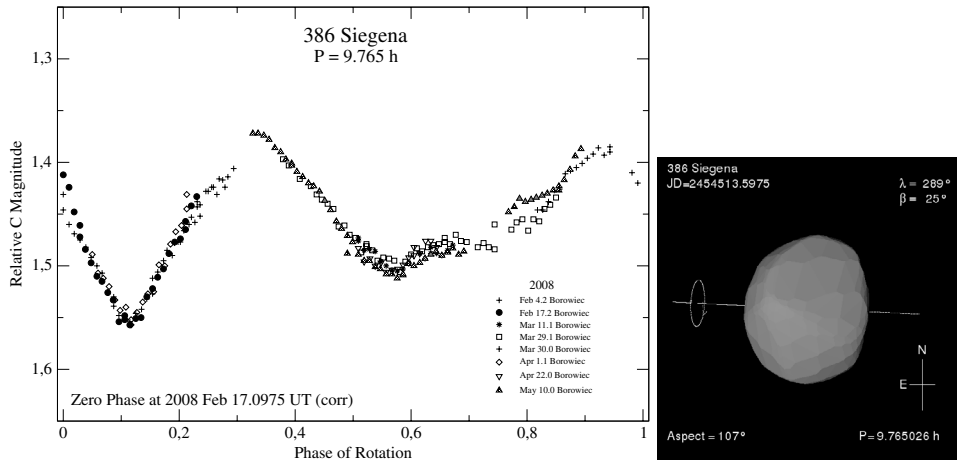


Fig. 42. Composite lightcurve of (386) Siegena in 2008 with the orientation of model 2 for the zero phase.

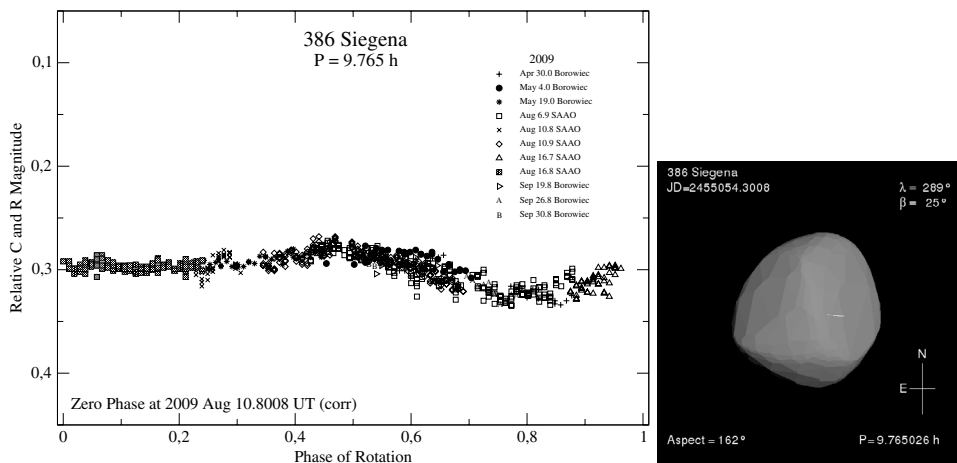


Fig. 43. Composite lightcurve of (386) Siegena in 2009 with the orientation of model 2 for the zero phase.

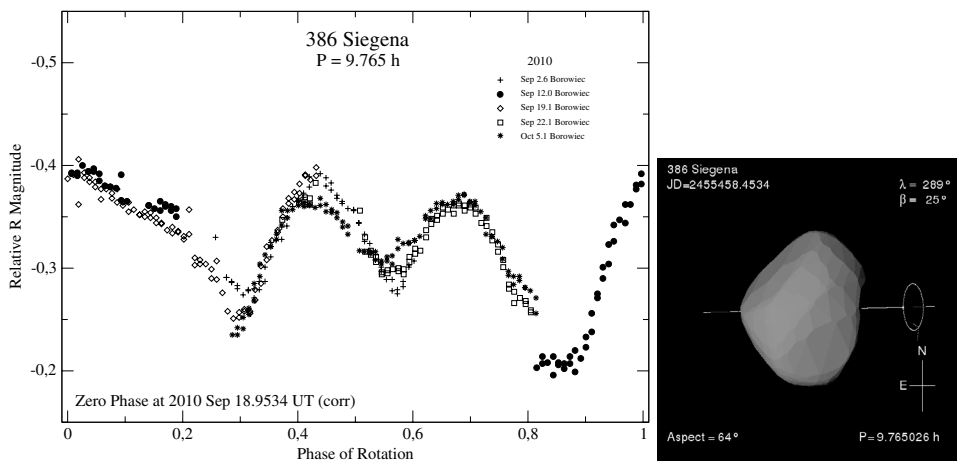


Fig. 44. Composite lightcurve of (386) Siegena in 2010 with the orientation of model 2 for the zero phase.

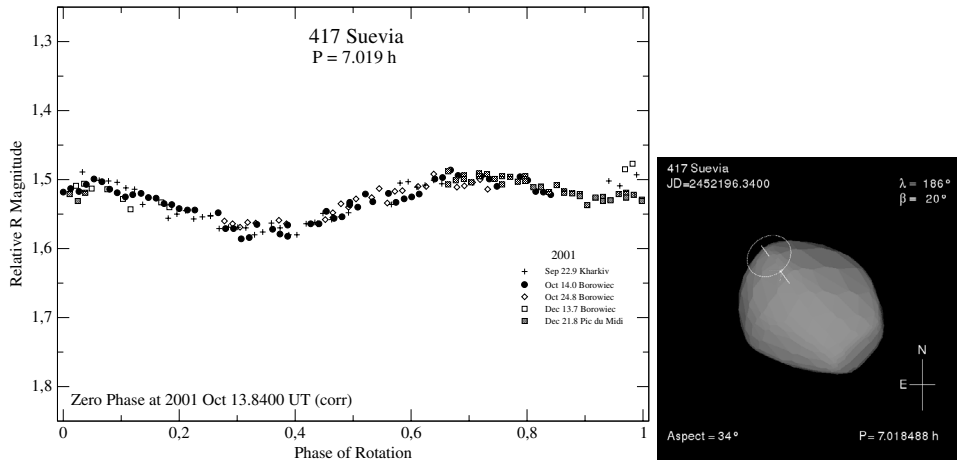


Fig. 45. Composite lightcurve of (417) Suevia in 2001 with the orientation of model 2 for the zero phase.

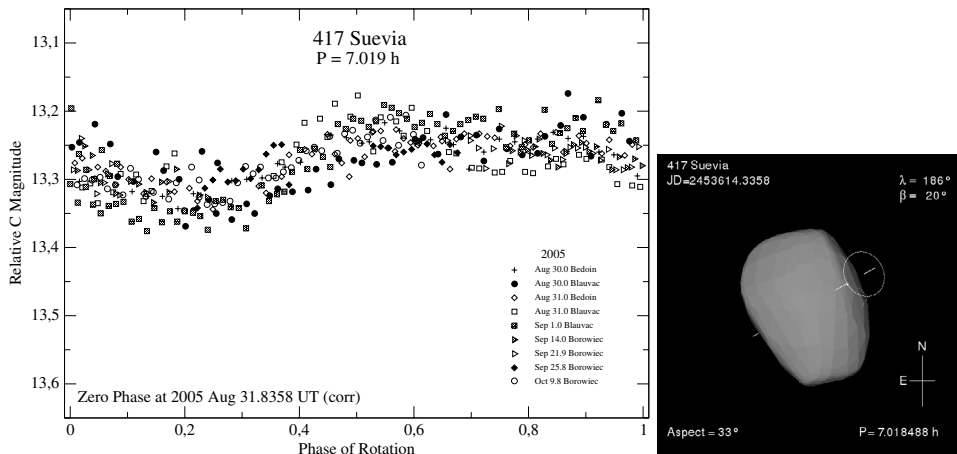


Fig. 46. Composite lightcurve of (417) Suevia in 2005 with the orientation of model 2 for the zero phase.

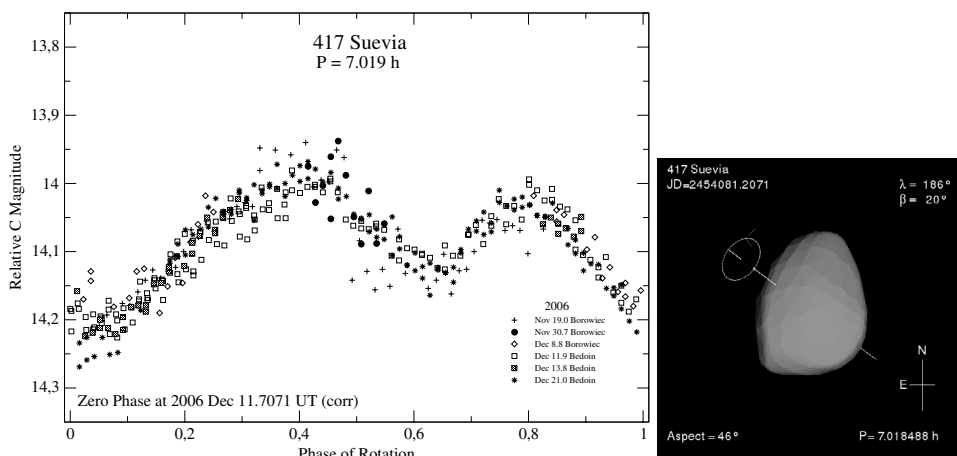


Fig. 47. Composite lightcurve of (417) Suevia in 2006 with the orientation of model 2 for the zero phase.

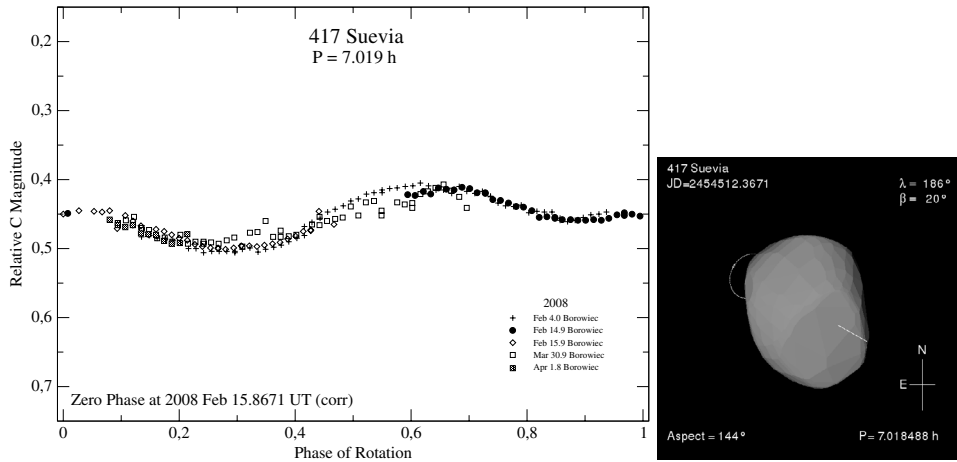


Fig. 48. Composite lightcurve of (417) Suevia in 2008 with the orientation of model 2 for the zero phase.

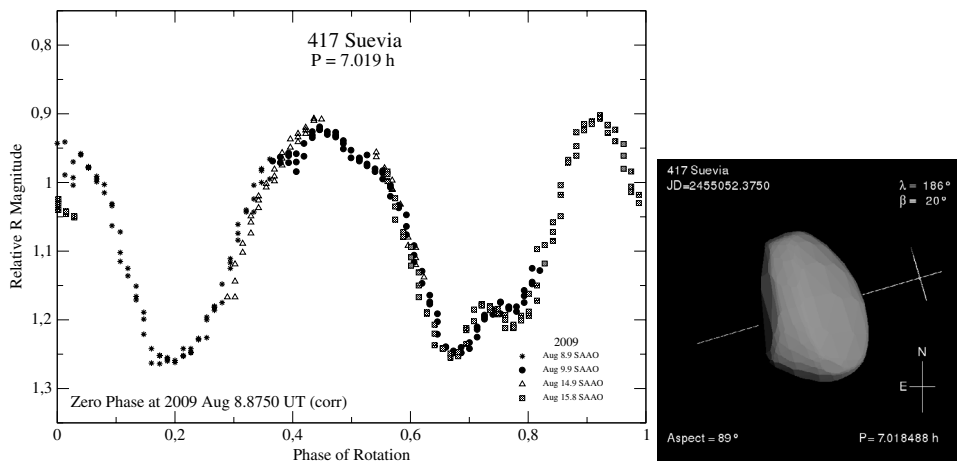


Fig. 49. Composite lightcurve of (417) Suevia in 2009 with the orientation of model 2 for the zero phase.

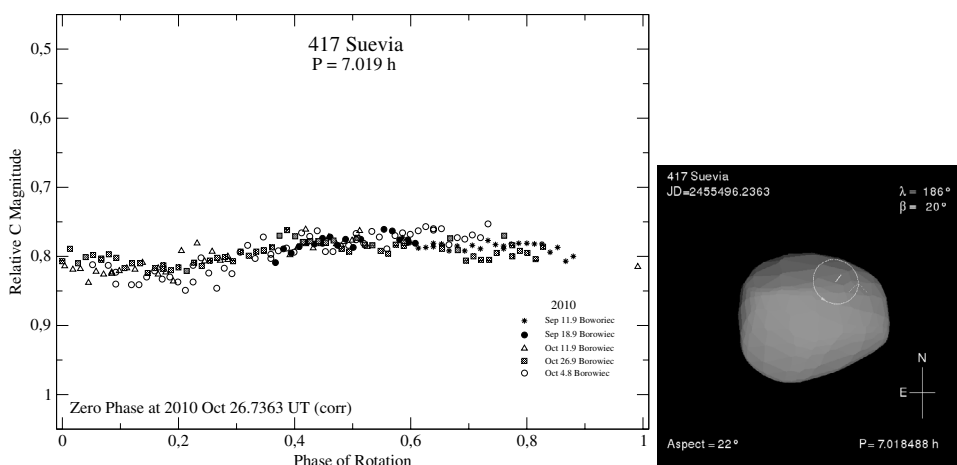


Fig. 50. Composite lightcurve of (417) Suevia in 2010 with the orientation of model 2 for the zero phase.

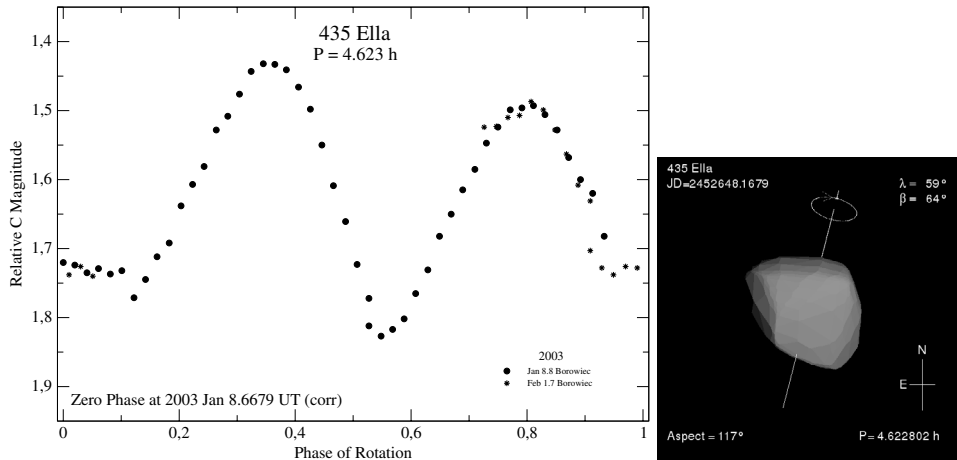


Fig. 51. Composite lightcurve of (435) Ella in 2003 with the orientation of model 1 for the zero phase.

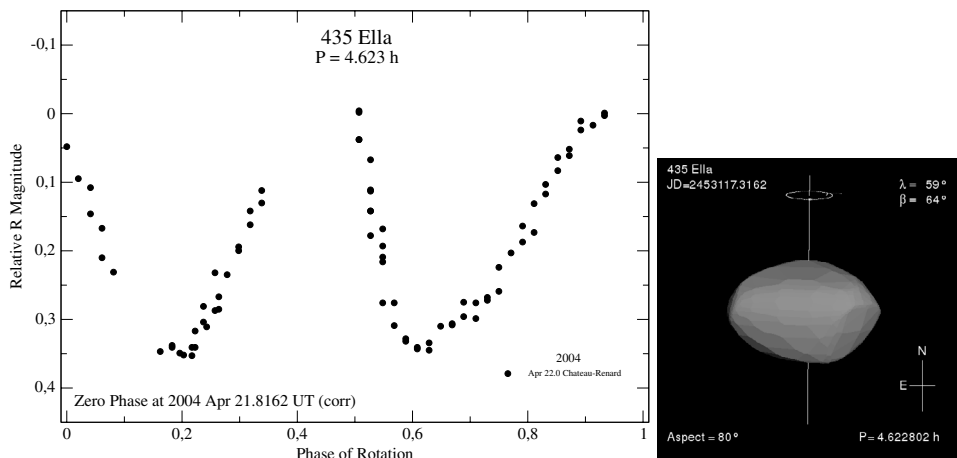


Fig. 52. Composite lightcurve of (435) Ella in 2004 with the orientation of model 1 for the zero phase.

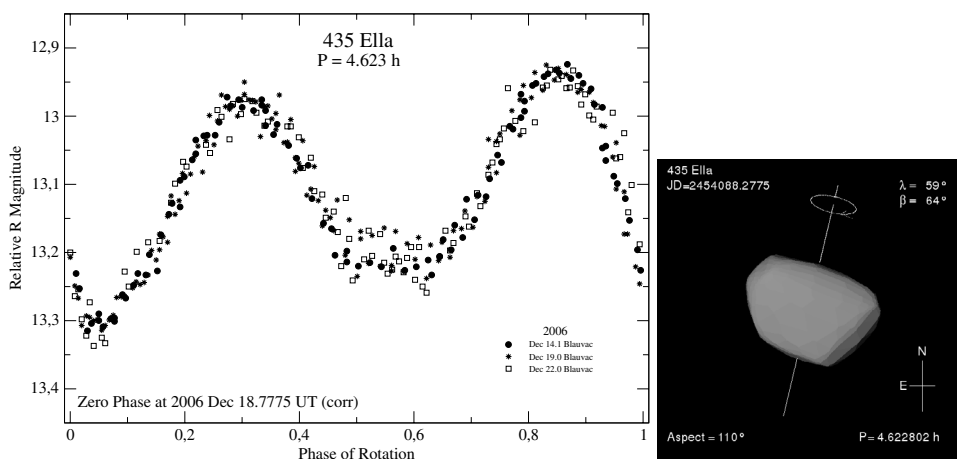


Fig. 53. Composite lightcurve of (435) Ella in 2006 with the orientation of model 1 for the zero phase.

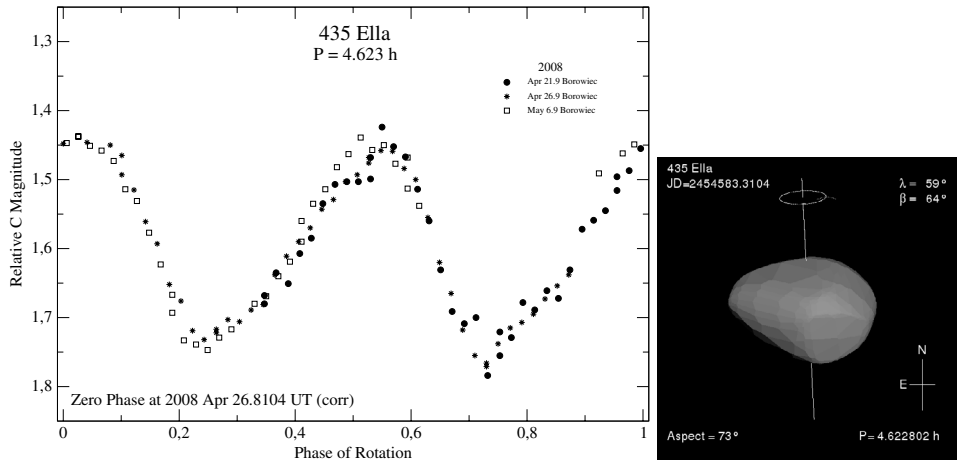


Fig. 54. Composite lightcurve of (435) Ella in 2008 with the orientation of model 1 for the zero phase.

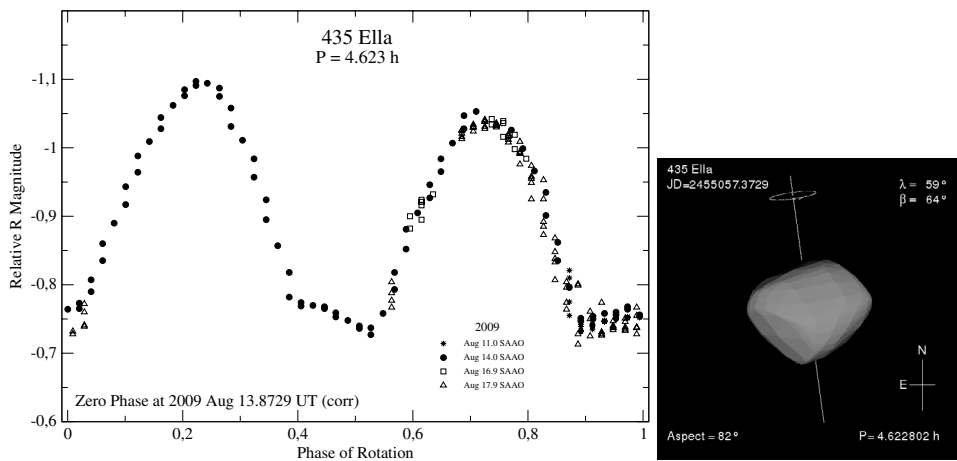


Fig. 55. Composite lightcurve of (435) Ella in 2009 with the orientation of model 1 for the zero phase.

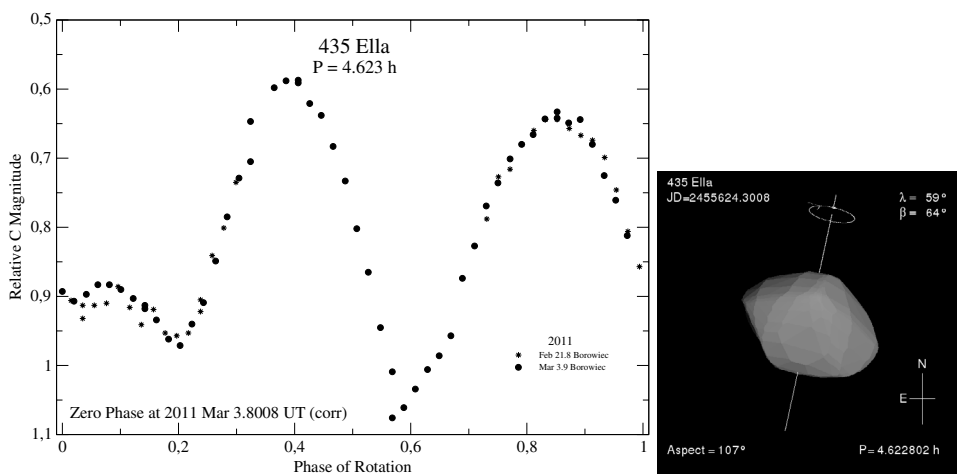


Fig. 56. Composite lightcurve of (435) Ella in 2011 with the orientation of model 1 for the zero phase.

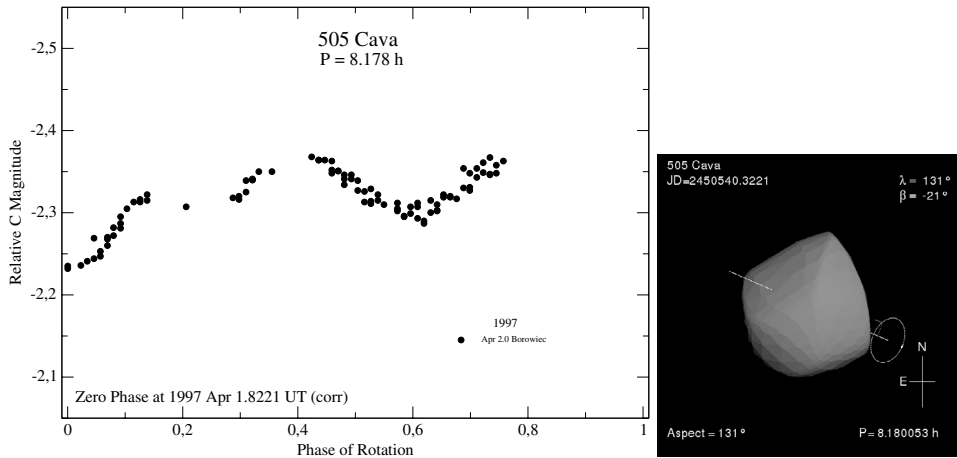


Fig. 57. Composite lightcurve of (505) Cava in 1997 with the orientation of model 1 for the zero phase.

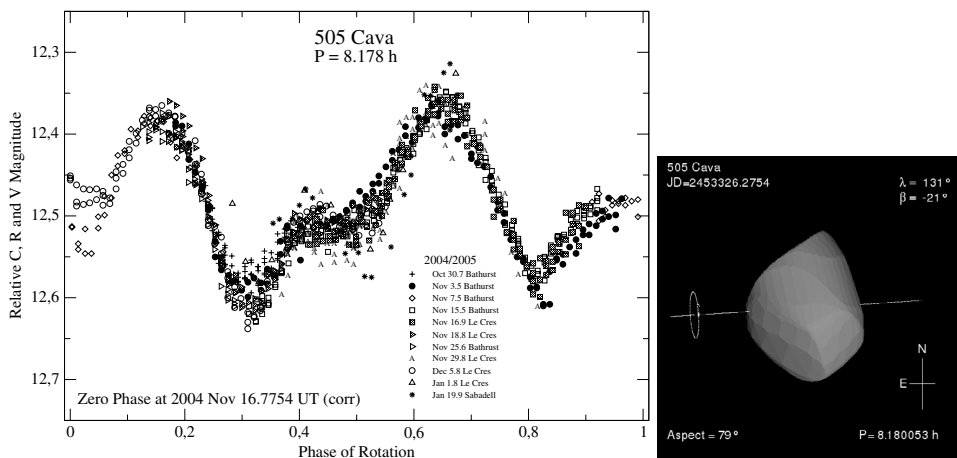


Fig. 58. Composite lightcurve of (505) Cava in 2004/2005 with the orientation of model 1 for the zero phase.

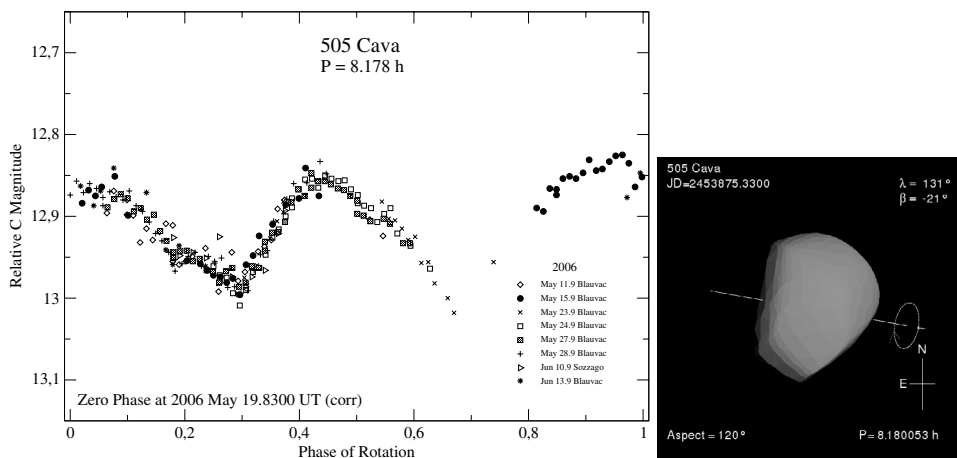


Fig. 59. Composite lightcurve of (505) Cava in 2006 with the orientation of model 1 for the zero phase.

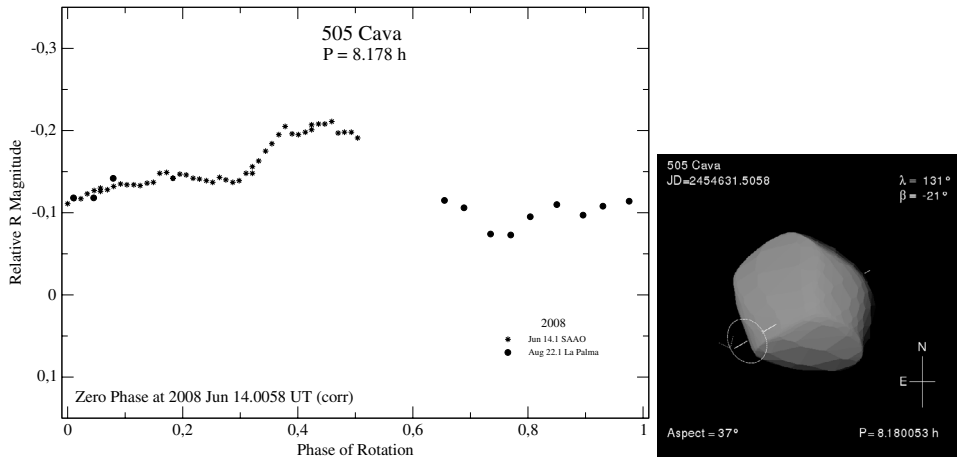


Fig. 60. Composite lightcurve of (505) Cava in 2008 with the orientation of model 1 for the zero phase.

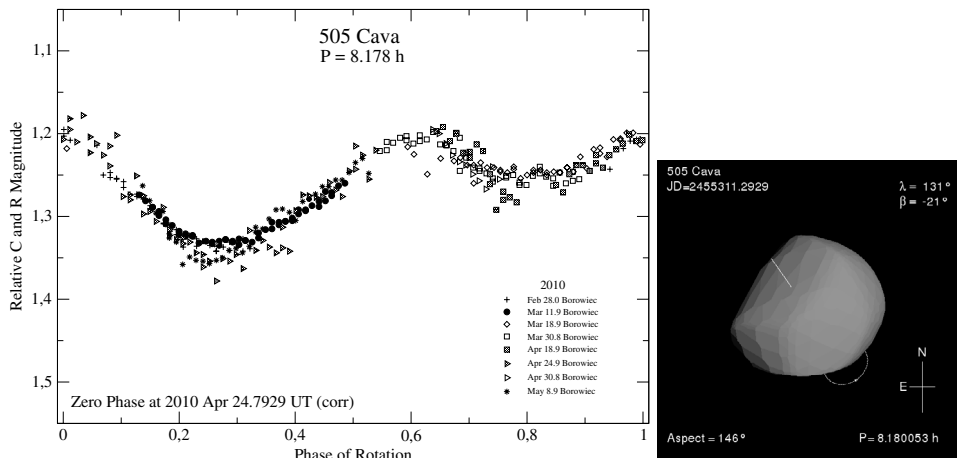


Fig. 61. Composite lightcurve of (505) Cava in 2010 with the orientation of model 1 for the zero phase.

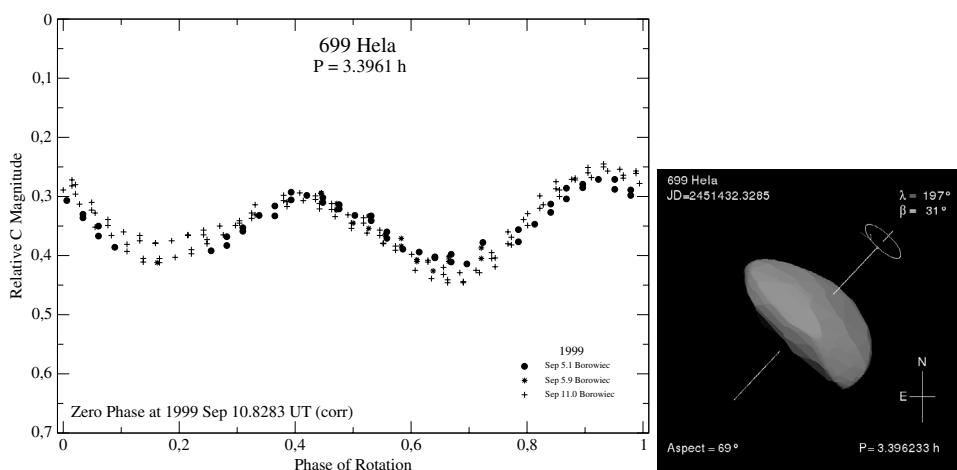


Fig. 62. Composite lightcurve of (699) Hela in 1999 with the orientation of model 2 for the zero phase.

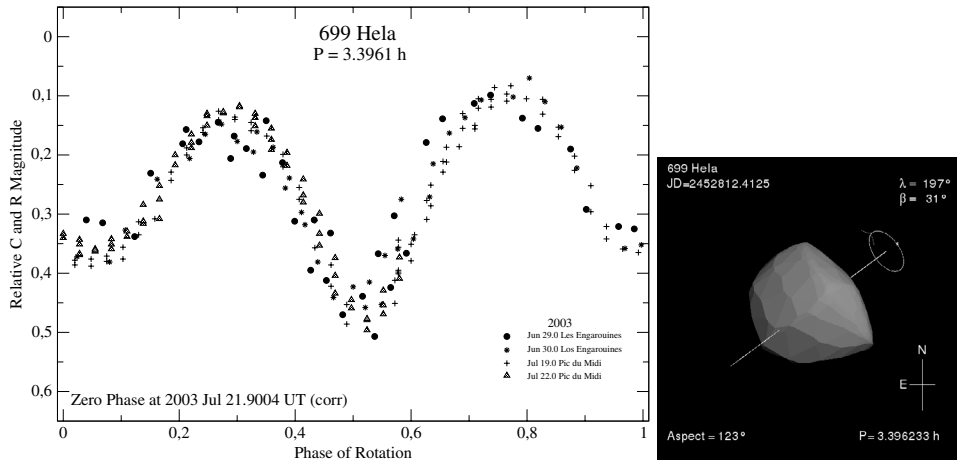


Fig. 63. Composite lightcurve of (699) Hela in 2003 with the orientation of model 2 for the zero phase.

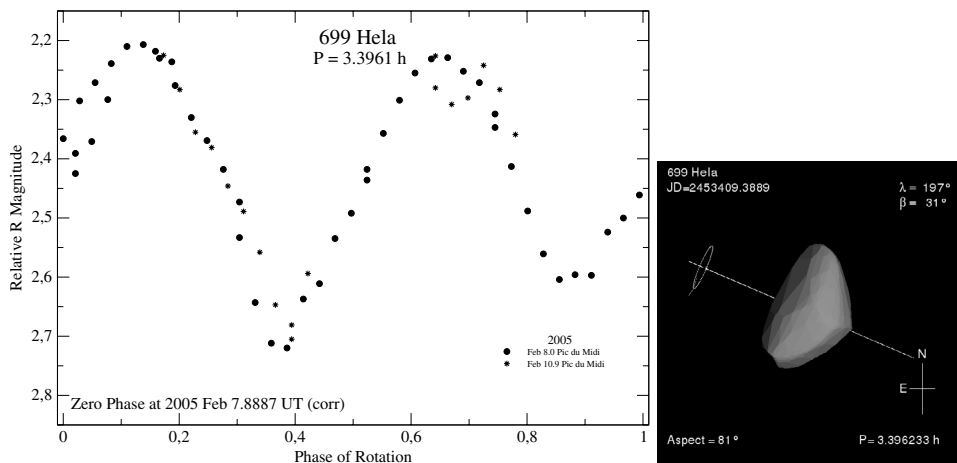


Fig. 64. Composite lightcurve of (699) Hela in 2005 with the orientation of model 2 for the zero phase.

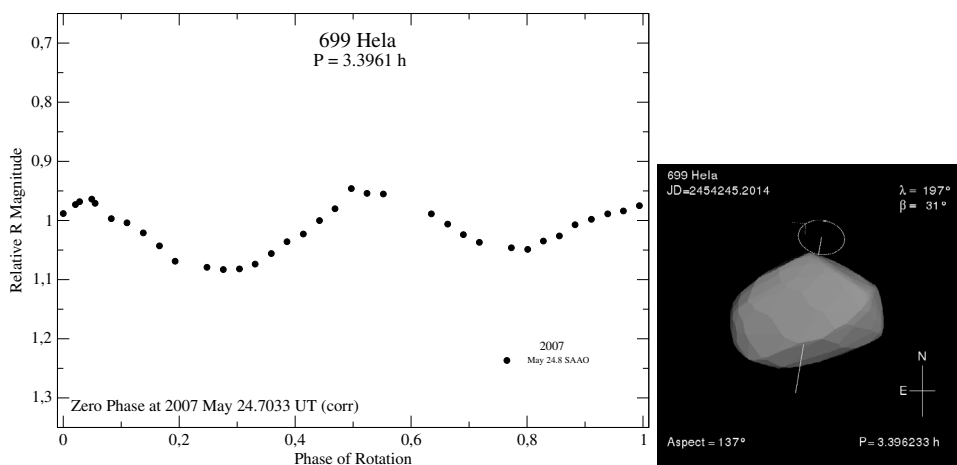


Fig. 65. Composite lightcurve of (699) Hela in 2007 with the orientation of model 2 for the zero phase.

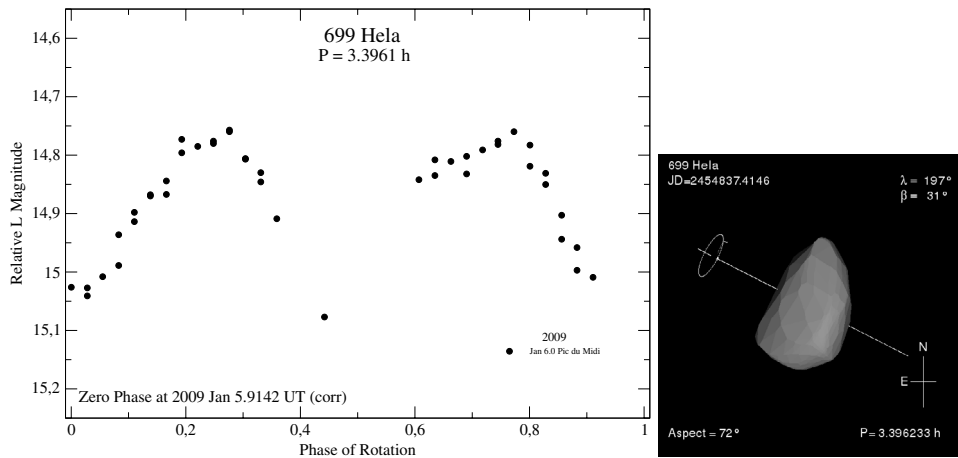


Fig. 66. Composite lightcurve of (699) Hela in 2009 with the orientation of model 2 for the zero phase.

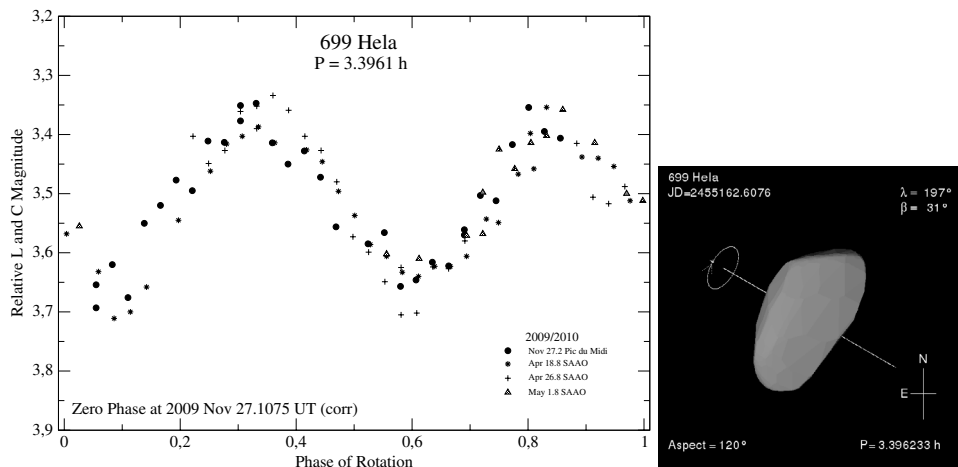


Fig. 67. Composite lightcurve of (699) Hela in 2009/2010 with the orientation of model 2 for the zero phase.